Journal of Earth and Atmospheric Research

LINEAMENTS AND STRUCTURES AS INDICES OF MINERALIZATION IN PARTS OF SOUTHEASTERN NIGERIAN SEDIMENTARY BASIN

[1]Okiyi, I. M., [2]Selemo, A. I.; [3]Ibeneme, S. I.; [4]Obioha, E. Y.; [5]Olorunfemi, M. O. and [6]Adikwu, S. O.

[1,2,3,4 & 6]Department of Geology, Federal University of Technology, Owerri Nigeria;
[5]Department of Geology, Obafemi Awolowo University, Ile-Ife, Nigeria,

Article History
Received: 01-12-20
Accepted: 24-03-21

Keywords:
Airborne Magnetic Data, Remote Sensing Data, Lineaments, Basement Depths, Mineral Prospect.

ABSTRACT

Digital processing, analysis and interpretation of twelve sheets of high resolution airborne magnetic and five scenes of Landsat 8 remote sensing data of parts of Southeastern Nigerian sedimentary basin were carried out with a view to evaluating magnetic source depths, map and quantify lineaments and determine trends of sub-surficial structural attributes which could have been involved in ore genesis and yielding regimented mineral colonies within the study area. Reduction to Equator and Vertical Derivative filters were applied to the residual airborne magnetic data to centre anomaly peaks over causative bodies, define shapes and edges of magnetic sources and map magnetic lineaments. Fast line-in-sight atmospheric analysis for spectral hypercube (FLAASH) and subsequent post FLAASH band maths were applied to the remote sensing data to generate the surface reflectance data from which ratio composite and lineament maps were generated. Results show dominant NE-SW and E-W lineament trends from Landsat and Magnetic data with subordinate NW-SE trend. The Vertical Derivative map revealed boundaries of mafic intrusive and inclusions which most likely controlled by the trends of deep-seated magnetic lineaments. Alteration zones, lithological boundaries and possible geologic models in the study area were revealed by Sabin's ratio map constituted by three ratio composites of 4/2, 6/5 and 6/7. The 3D Euler Deconvolution and Magnetic Vector Inversion modelling depth estimate filters established depths to and geometry of subsurface magnetic structures. Results reveal shallow to deep-seated structures in the depth range of 80 m asl to >7 km bsl. Deep-seated fractures and fissures must have aided development of veins, lodes of intrusive or ore bodies. Cylindrical sills, inclined dykes, sparse nodules and spheres were identified from some probed windows of the RTE-TMI map, indicating that the study area is a viable mineral prospect environment.

Correspondence: millijey@yahoo.com

1.0 INTRODUCTION

Geophysical investigation is reliant on variations in the physical properties of host rocks relative to geological targets such as ore deposits. Contrasting properties as observed in hydrocarbon bearing oil traps within host sedimentary formations, dykes or sills hosting valuable minerals or base metal deposits within host basement rocks, water accumulation and flow within and along fractures making up groundwater drainage systems, within fresh host rocks yield such contrasts (Telford et al., 1990). Depending on the physical property of the target that is being investigated, such as reflectivity,

magnetic susceptibility, density, elasticity, radioactivity, geothermal gradient, and resistivity/ conductivity (Adagunodo *et al.*, 2015), different geophysical methods can be adopted on land, on the sea or from aircrafts or satellites in airborne and remote sensing surveys. Where a large area is needed to be surveyed and there are challenges with accessibility, remote sensing is favoured because it provides a synoptic view over large area (Kolawole *et al*., 2012).

Sharma (1987) observed that of all geophysical methods, the magnetic method is the oldest, simplest and most widely used for locating hidden ores and structures associated with mineral deposits. The principles of magnetism help understand the various modes of responses of earth materials to magnetic field (Dobrin and Savit, 1988). Anomalies in the local geomagnetic field arising from magnetization by earth's magnetic fields and remanence are measured (Glatzmaier and Roberts, 1995). Trends of magnetic features, that most often have semblance to the trend of the overlying sediment and sedimentary structures, are to a large extent controlled by basement tectonics. Both active and passive remote sensing systems detect and record energy signals from earth surfaces and/or from the atmosphere (Schowengerdt, 2007) by operating in or above the earth's atmosphere within the principal sensing regions of the visible, reflected near-infrared, thermal infrared, and microwave radar regions of the electromagnetic (EM) spectrum (Abdulrahman, 2010). Geologic lineament mapping from airborne magnetic and remote sensing data has been found useful in engineering projects, especially in site selection for civil engineering construction works (dams, bridges, roads), seismic and landslide risk assessment, mineral exploration, hot spring detection and hydrogeological investigations (Kolawole *et al*., 2012; Abuzied and Alreface, 2017 and Ilugbo and Ozegin, 2018).

The Lower Benue Trough (LBT), originates from earth's dynamicity of the convective cells within the mantle (mantle dynamics) which resulted to the drift of South American and African Continents and the formation of an aulacogen (failed rift/trough) (Grant, 1971). This major geological structure extends about 1,000 km northeast from the Bight of Benin to Lake Chad and is about 150 km wide (Grant, 1971). The NE-SW trending Cretaceous, elongated structure contains as much as 6,000 m thick Cretaceous-Tertiary sediments, including those predating the middle Santonian which have been compressionally deformed, faulted, and uplifted in several places (Benkhelil, 1989). These geological processes, which led to the formation of the Trough, made it favourable for geothermal and mineral resource enrichment. The importance of aulacogens as suitable environments for base-metal deposits has been observed by Sawkins (1976), Olade and Morton (1980) and Robbins (1983).

Others, including Mirianrita *et al*.(2015), Anyanwu and Mamah (2013), Onuba *et al*.(2011) and Obi *et al*.(2009), have also indirectly estimated the sedimentary thicknesses of the Cretaceous sediment enriched Benue Trough by determining the depth to the magnetic basement based on interests in the spectra of oil maturation investigation, delineation of intrusive dykes for quarry purpose, base metal deposits for solid mineral exploration, hydrothermal flow from magnetic basement sources through geothermal gradient studies. Several authors in time past had engaged in researching on occurrence of individual deposits in the southeastern Nigerian sedimentary basin. These include; Tattam (1930), Orajaka (1965),

Nwachukwu (1974), Olade (1976), Ezepue (1984) who investigated Pb-Zn mineralization in Abakaliki; Etim *et al*.(1988), Egboka and Uma (1986), Uma *et al.* (1990), Uma and Loehnert (1992), Omada and Ike (1996), Uma (1998), who studied brines and Farrington (1952), Olade (1978), Umeji and Can Vachette (1983) who researched on igneous bodies/intrusive.

Minerals occur in cracks, crevices, faults, fractures, joints, shear zones and breccia of igneous and metamorphic rocks. Such minerals include gold, tin, copper, zinc, iron, cassiterite, and lead (Ananaba and Ajakaiye, 1987 and Evans, 1995). Structure-controlled mineralisation is amenable to geophysical delineation either directly through their physical characteristics such as density, resistivity/conductivity, magnetic susceptibility, and elastic property, most especially when the ores occur in massive form or indirectly by mapping their hosts such as veins, faulted, fractured, sheared and jointed zones (Doyle, 1990). Remote sensing/satellite imageries and geophysical prospecting methods (magnetic and gravity) have found useful applications in the mapping of potential ore bearing linear geological strutures (Nash *et al*., 1980; Goetz and Rowan, 1981; Peters, 1983; Drury, 1986, 1993; Rowan and Bowers, 1995; Hoover *et al*., 1995; Adagunodo *et al*., 2015; Akinlalu *et al*., 2018 and Bamidele, 2020).

This study, therefore, intends to engage high resolution airborne magnetic and remote sensing data to estimate depths to magnetic basement, map lineaments and lineament density and trends of sub-surficial structural attributes that are suspected to be ore genesis related with a view to yielding regimented mineral colonies within parts of the southeastern sedimentary basin.

2.0 DESCRIPTION OF THE PROJECT AREA

2.1 Geographic Location, Drainage, Vegetation and Climate

The 36,300 km^2 study area is located between Latitudes 5° 30' N and 7°00' N and Longitudes 7° 00' E and 9° 00' E encompassing Enugu and Ebonyi States and parts of Anambra, Imo, Abia, Akwa Ibom and Cross Rivers States; within the southeastern sedimentary basin of the LBT (Figure 1).The area is directly bounded by Kogi State to the North, Delta and Edo to the West and Bayelsa and Rivers States to the South and to the East by the Cameroon. The area is well drained by Cross River and its tributaries. The drainage pattern is dendritic. The area has ever green vegetation with eastern prototype mixtures of semi-savannah grasslands, forests and swamps. The climate is the tropical rainforest type with annual precipitation in excess of 2,000 mm (80 in) in the South and over 3000 mm (120 in) in the far South East (Iloeje, 1981 and Encarta, 2009).

2.2 Geology

The stratigraphy of the study area from the bottom consists of the marine Neocomian-Albian Asu River Group sediments composed of shales and localized sandstones, siltstones and limestones (Onu, 2017)(Fig.2). Overlying the Asu River Group is the Cenomanian-Turonian Nkalagu Formation consisting of New Netim Marl's black shales, limestones and siltsones. It is a 900 m thick fossil-rich bluish grey and bedded Awgu Shales with fine-grained carbonaceous limestone beds in close association with subordinate limestone and calcareous sandstones and interfingering regressive sandstones of the Agala and Agbani Formations (Ezeaku Formation of the Cross River Group). There was also contemporaneous silting sequence of unconformably deposited sandstones, limestones, shales and calcareous sandstones of the Odukpani Formation on the folded basement rocks of the Calabar Flank during the Late Albian. There was a hiatus, the

depo-centre of the depo-valley shifted westwards and it became an area of derivational sediments within Abakaliki-Benue Trough (Afikpo Syncline) and Anambra Basin (Obaje, 2009).

The Santonian time was a period of non-deposition which had more compressive forces that led to the folding of the entire sedimentary rocks, producing folds and synclines in the NE-SW trend (Obaje 2009).There were major westward displacements of depositional axes leading to the formation of post-deformational sequences in the LBT, constituting the Anambra Basin (Odoma *et al.,* 2013). Commencing the sedimentation in this basin are sequences of bluish to dark grey shales and mudstones locally intercalated with sandy shales, thin sandstones and shaly limestone beds constituting the brackish marsh and fossiliferous pro-delta facies of the Campanian-Early Maastrichtian Enugu and Nkporo Formations (lateral equivalents). These grade laterally to sandstones of Owelli and Afikpo Formations of the Anambra Basin. Most parts of the Anambra Basin were overlain by Lower Maastrichtian sandstones, shales, siltstones, mudstones and inter-bedded coal seams of the Deltaic Mamu Formation, N-S from the Calabar flank, during an overall regression of the Nkporo cycle. Sedimentation from the converging littoral drift cells reflect on the Cretaceous tidal red earth sands of Ajali Sandstone which are poorly sorted, false-bedded and friable sandstones with great thickness marking the height of regression at a time when the coastline was still concave. Overlying the Ajali Formation is the Nsukka Formation.

The Imo shales alongside the Nsukka Formation mark the onset of another transgression in the Anambra Basin during the Paleocene. They are overlain by tidal Nanka Sandstone of Eocene age (Fatoye *et al*., 2014), denoting another return to regressive conditions. This is evident from well-exposed, strongly asymmetrical sandwaves which suggest the predominance of flood-tidal currents over weak ebb-reverse currents. In turn, Nanka Sandstones are overlain by Tertiary units of sandstones, shales laden with significant amount of organic matter and lignite beds of Oligocene/Miocene Ogwashi-Asaba Formation All constitute the proto-Niger Delta Eocene to Recent sequences in the subsurface (Fatoye & Gideon, 2013).The study area occurs within the described formations above and has some basins occurring within it, such as the Anambra Basin, Afikpo Basin, Mamfe Basin and Niger Delta Basin. The Mamfe basin has its adjoining areas to the Cameroon Republic. The geology of the study area is elaborated in Figure 2.

3.0 METHODOLOGY

3.1 Materials

Twelve (12) airborne magnetic data sheets which include Nsukka 287, Igumale 288, Ejekwe 289, Ogoja 290, Udi 301, Nkalagu 302, Abakaliki 303, Bansara304, Okigwe 312, Afikpo 313, Ugep 314, and Ikom 315 were used. Five Scenes of Landsat 8 data; Landsat_8_Path_187_ROW_55_2019, Landsat_8_Path_187_ROW_56_2019 Landsat_8_Path_189_ROW_55_2019, Landsat_8_Pat_187_ROW_56_2019, and Landsat_8_Path_188_ROW_55_2019 were downloaded from USGS (United State Geological Services) Google Earth Explorer and opened in an environment for visualizing images (ENVI 5.1). The files were transported from ENVI to ArcGIS in order to assign bearings because ENVI 5.1 doesn't make provisions for such. The need for a paradigm shift to the solid mineral sector made the Federal Government of Nigeria to embark on provision of quality geosciences data through airborne geophysical survey programme hence FUGRO was contracted between 2005 and 2007 to carry out a Phase 1 survey programme with 45% national coverage, including the Benue

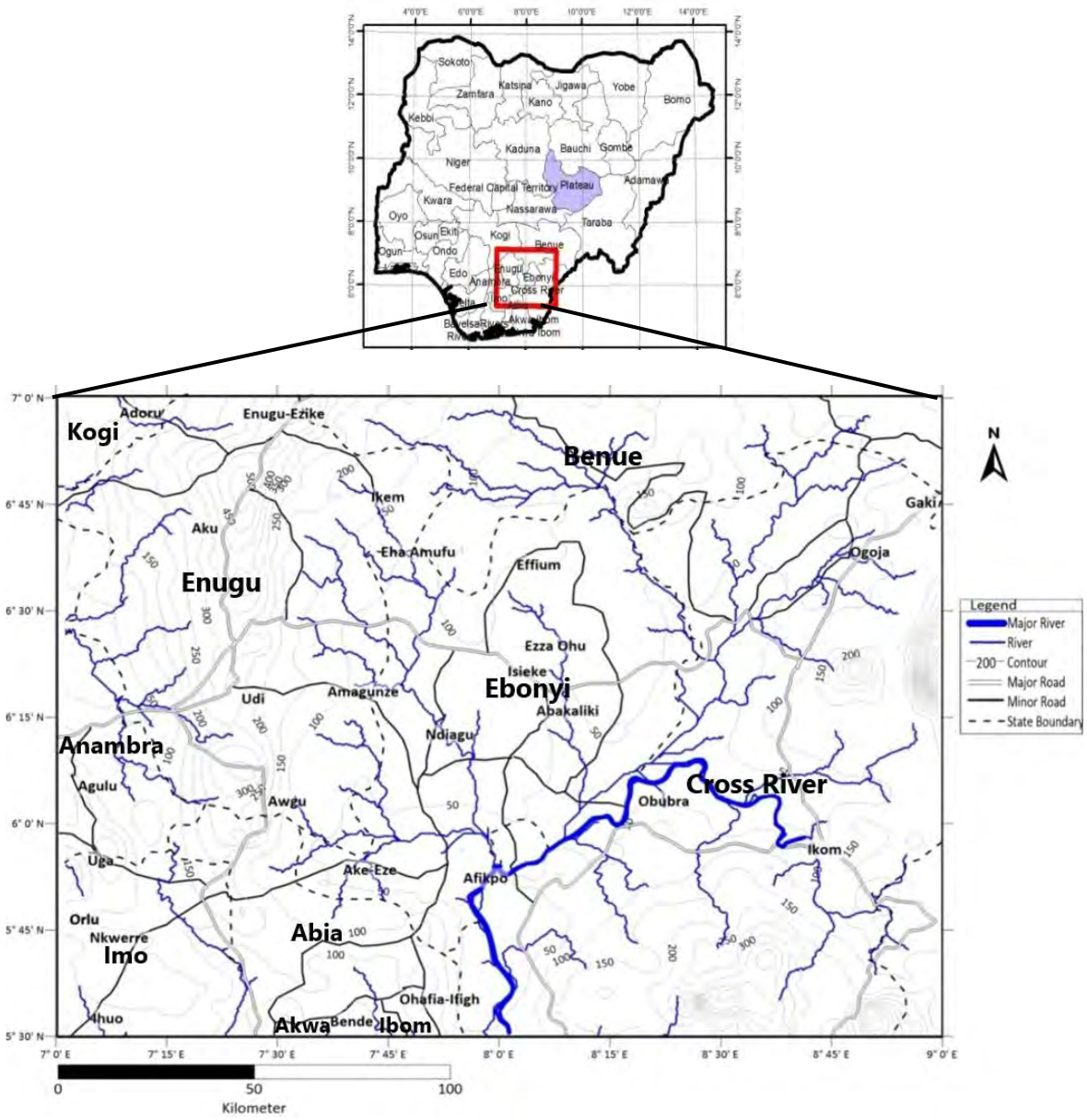


Figure 1: Topographical Map of the Study Area (Digitized from Ryan et al. (2009).

Trough, parts of southwest, middle belt and up to northwestern regions of the country under the supervision of the Nigerian Geological Survey Agency (NGSA). The World Bank through Sustainable Management of Mineral Resources Project (SMMRP) also commissioned FUGRO for phase II airborne survey between 2007 and 2010, covering 55% of Nigeria's landmass. These two phases included magnetic, radiometric, gravity and electromagnetic domains flown at 500 m line spacing, 80 m terrain clearance, generating a 2 million total line-km data in a NE-SW direction and recorded at 0.1s interval. The airborne magnetic data were sourced from the Nigerian Geological Survey Agency (NGSA) and the International Geomagnetic Reference Field model of 2015 referenced to world geodetic system was used to remove the geomagnetic gradient. The aeromagnetic data were geo-referenced to the Universal Transverse Mercator

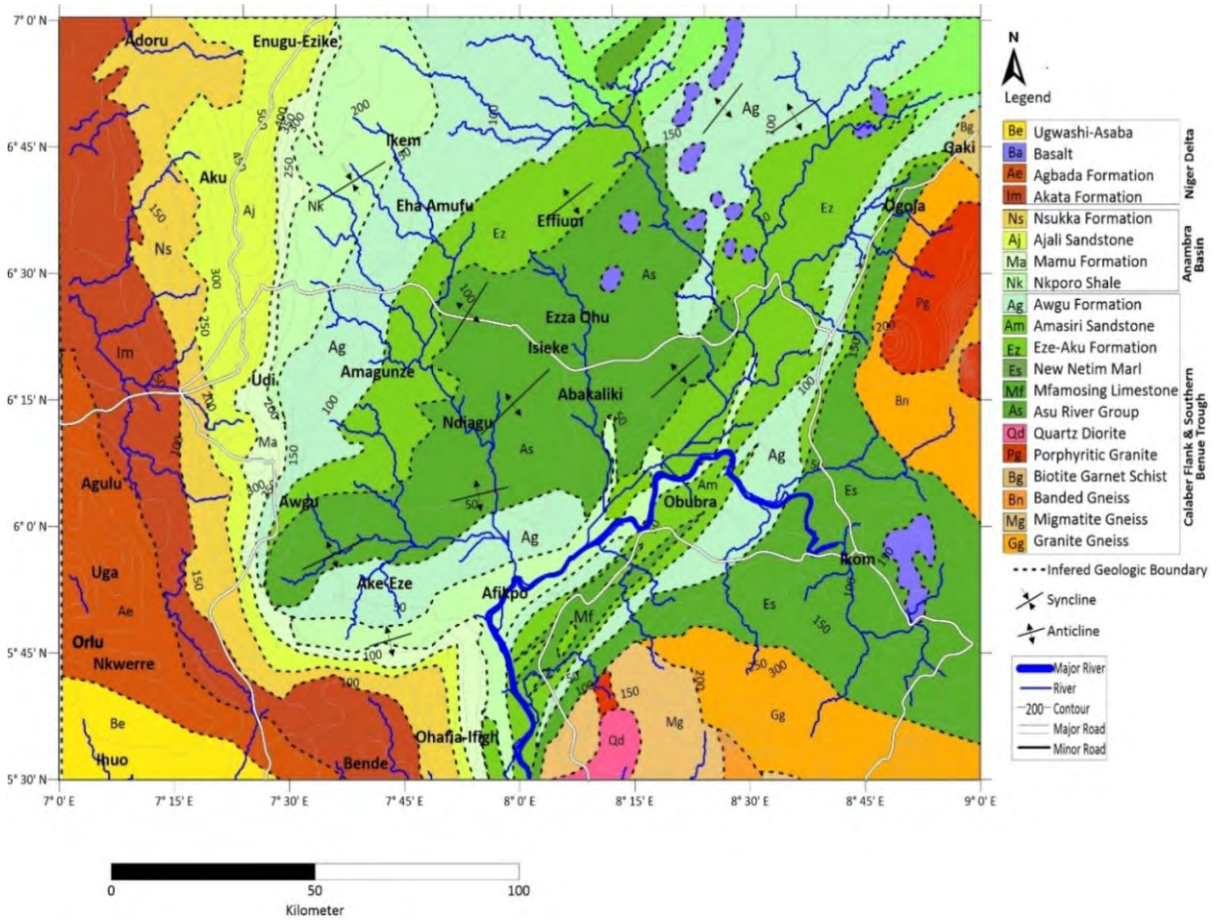


Figure 2: Geologic Map of the Study Area {(Digitized from Geologic Map of Nigeria, Nigerian Geological Survey Agency, 2010)}

coordinate system to make effective comparison with geological map of the area.

3.2 Methods of Study

3.2.1 Remote Sensing

Surface Reflectance and Composite Maps

Atmospheric correction was carried out on the digitized remote sensing data to remove the effects of reflections from haze or vapor and those reflections that didn't eventually get to the earth's surface (atmospheric reflection). This fast line-in-sight atmospheric analysis for spectral hypercube (FLAASH) and subsequent post FLAASH band maths were applied to generate the surface reflectance data. There was no need for radiometric correction in Landsat 8 because the correction had already been done on the sensors. All the individual scenes making up the extent of

Table 1: Common Band Combinations Applied to Landsat 8 (Adapted from Butler, 2013)

Band Colours	Band Combinations
True/Natural Colour	432
False Color (Urban)	764, 753, 453
Colour Infrared (Vegetation)	543
Agriculture	652
Geology	762
Atmospheric Penetration	765
Healthy Vegetation	562
Land/Water	564
Natural Vegetation With Atmospheric Removal	753
Bathymetric	431
Shortwave Infrared	754, 764
Vegetation Analysis	654

the study area were mosaicked together to produce a single dataset from which the exact perimeter of the study area was resized and all unwanted parts were filtered off. This was done by clicking and subjecting the required mosaic to some process involving export of the mosaic as a TIF file of the study area to ENVI environment. The ENVI environment has an existing algorithm to compute calculations unlike ArcMap which needs input of formula and computation, hence, atmospheric correction involving radiometric calibration and dark subtraction was done to obtain a mosaic picture. The sun angle correction was also conducted on the mosaic as represented in equation 1.

Sun angle correction =

$$\frac{[(0.0002 \text{ x band}) - 0.1}{\text{Sin(Sun Elevation)}} \quad (1)$$

where sun elevation = 50.00589923

The Surface Reflectance Data/True Colour Composite of the study area gives reflection of earth's surface material (aggregate of top 15cm of the earth). The Red Green Blue (RGB) bands of spectra has 4, 3, 2 assigned respectively to the EM spectra because the Landsat scene must be represented in these three (3) colours (RGB).

Band Rationing and Combination

Imputation of bands for band rationing was done in ENVI environment where numerator and denominator values were inputted and exported to ARCMap environment for embellishment or fine-tuning of finalized maps. Colour combination is a typical way for displaying multi-spectral imagery by attributing the three primary colours (red-green-blue) to three chosen bands that are simultaneously combined (Prost, 2014). Band rationing accentuates spectral characteristics of certain materials or minerals by rationing their reflectance band over their absorption band .Most common combinations are displayed in Table 1 and especially 6-5-2, 6-5-3, 7-5-2, 7-5-3 and 7-6-5 Landsat-8 OLI bands for geological remote sensing (Rajesh, 2004). In this study, band ratios; 4 on 2, 6 on 5 and 6 on 7 were used, as they constituted the Sabin's Ratio. Ali and Amin (2014) used the Sabin's ratios (4/2, 6/7 and 6/5 as RGB) for lithological mapping and delineation of hydrothermal alteration zones.

Lineament Extraction

Lineaments usually appear as straight lines (edges) on satellite images (O'Leary *et al.*, 1976); which are contributed by tonal differences of surface materials. Lineament extraction technique remains a veritable tool in the identification of crevices relevant to ore accretion. The first stage involves selection of initial input data for lineament extraction irrespective of the fact that lineaments can as well be extracted from aerial photographs or geophysical data. In this study, the satellite image is preferred for this application and the extraction of lineaments from satellite images precedes a final lineament map generation. Lineament extraction in this study is automatic. It involved contrast stretching of mosaicked scenes of surface reflectance data, followed by image analysis in MVI and Rockwork environments. The data were further taken to PCI Geomatica platform for image filtering and subsequently to ArcGIS environment where lineament extraction was done and lineament density map, produced. Lineament map was also generated from aeromagnetic data as discussed in the next section. Satellite image derived lineaments are superficial while aeromagnetic derived lineaments are generally deep-seated. The integration of both lineaments will give a composite lineament map for the study area.

3.2.2 Aeromagnetic Survey

Reduction to Equator

The Total Magnetic Intensity (TMI) map usually given by the NGSA is virtually a residual map having removed a regional magnetic field of 32000nT from the observed data set. Due to Nigeria's nearness to the magnetic equator than the poles (N and S poles), it is preferred to reduce the TMI data to that at the magnetic equator (RTE). RTE map centers anomaly peaks over their sources and simplifies interpretation as well (Sheriff, 1991; Sharma, 1997). The production of the RTE gridded map enables other enhancement routines for various studies.

Vertical Derivatives
First Vertical Derivative (FVD)

This filter is commonly applied to total magnetic field data to enhance shallow geological sources by enhancing the high frequency (wavenumber) components of the anomaly spectrum. Equation 2 represents the generalised equation for the vertical derivatives (GEOSOFT Inc., 2010) and is given as;

$$L(\omega) = \omega^n \qquad (2)$$

where ω = wave number and
n = order of differentiation;
L= anomaly spectrum

The changes in values of wave number components differentiates the FVD (where n=1) from SVD (where n=2) and enables subtle transitions in lithological changes to be deduced within different lithologies, enhance linear features like dykes, sills, geologic contacts, faults, fractures, clearer resolution of lithologic boundaries and distinguish hyperbasal materials from felsic rock forming minerals.

Second Vertical Derivative (SVD)

The Second Vertical Derivative filter enhances edge detection and enables mapping of geological contacts, faults, fractures and lithological boundaries using the zero contour lines (Nabighian *et al.,* 2005, Bamidele, 2020).

Euler Deconvolution

The standard 3D Euler Deconvolution technique is based on Euler's homogeneity equation which relates the potential field (magnetic or gravity) and its gradient components to the location of the source with the degree of homogeneity N, which may be interpreted as a Structural Index (Thompson, 1982). The Euler's homogeneity equation is of the form:

$$(x - x_0)\frac{\delta T}{\delta x} + (y - y_0)\frac{\delta T}{\delta y}(z - z_0)\frac{\delta T}{\delta z} = N(B - T) \qquad (3)$$

Where (x_0, y_0, z_0) = the position of the magnetic source whose total field (J) is detected at (x,y,z); B = the regional magnetic field; N = the measure of the fall-off rate of the magnetic field and may be interpreted as structural index (SI).

The structural index (SI) is a measure of the rate of change with distance of a field or the fall-off rate of the field with distance from the source and the system uses a least square method to solve Euler's equation simultaneously for each grid position within a sub-grid (window). A square window, 10 by 10 is moved along each grid row and for a 10 by 10 window, there will be 100 equations at each grid point from which unknown variables of locations X, Y, Z and a background value B and their uncertainties (standard deviations) are obtained for a specified structural index. The 3D Euler Deconvolution of aeromagnetic data have been established and modified after Thompson (1982) for contacts, sills and dykes, horizontal cylinders and pipes and spheres, based on certain criteria or attributes. These afore-mentioned structures have structural indices of 0, 1, 2, 3 respectively. However, for this study a structural index of 0 was found to be applicable.

Magnetic Lineament Extraction

The magnetic lineaments were automatically extracted from the RTE-TMI data in OASIS MONTAJ environment. The CET Grid Analysis system analyzes the filtered texture of the RTE-TMI image to detect lineament along ridges and edges as well as regions of complex structures. The equator reduced data were loaded on MAGMAP and CET (Centre for Exploration Targeting) Grid Analysis menus. Texture analysis of lineations and measurement of their randomness were determined using the Standard deviation. For a window with N cells, whose mean value is μ, the standard deviation, σ, of cell values, X_1 is given by equation 4:

$$\sigma = \sqrt{\left[\frac{1}{N}\Sigma(X_i - \mu)^2\right]} \quad (4)$$

(Oasis montaj guide, 2012).

This overcomes inherent noise in the data and enhances lineation detection and smooth representatio]of degree of randomness. The lineations were vectorized and skeletonized using a scaled filterwavelength, filter scales and symmetry of robustness.

Magnetic Vector Inversion (MVI)

Magnetic vector inversion (MVI) is advancement in quantitative interpretation of magnetic data which has extended its utility to mineral exploration. MVI has found usefulness in providing effective approach to evaluating and investigating remanence and self demagnetization in multiple and complicated-shaped magnetic anomalies relating to mineralization (Liu *et al*., 2017 and Fournier *et al*., 2020). The inversion of geomagnetic field data was used in this study with the aim of determining the property and geometry of subsurface magnetic sources by automatically retrieving the distribution of subsurface magnetization or magnetic susceptibility from observed magnetic data. (Utsugi, 2019). MVI borders on magnetization distribution which is dependent on both direction and magnitude (Li, 2017) as summarized in the equation 5

$$\Delta T(\vec{r}) = \frac{\mu_0}{4\pi}\iiint_v^v J(\vec{r'})\hat{J}(\vec{r'}).\nabla^T\nabla\frac{1}{|\vec{r}-\vec{r'}|}.\hat{B}_0 dv' \quad (5)$$

Where J = magnetic polarization/magnetization, J(r̄) = magnitude and Ĵ = direction are unknown and Ĵ $=B_0$ when weak magnetization is assumed for susceptibility magnetization.

The generalized inversion uses 3D distribution of magnitude of magnetization or magnetization itself and it involves inversion amplitude data which equals length of anomalous magnetic field vector (equation 6). It recovers magnetization as a function of spatial position and accommodates ambiguity to maintain flexibility of algorithms and develop ways to solving problems associated with unknown magnetization direction.

$$B_a = |B_a| = \sqrt{B_{ax}^2 + B_{ay}^2 + B_{az}^2} \quad \text{(Li, 2017)} \quad (6)$$

where B_a = amplitude; B_{ax} B_{ay} *and* B_{az} = three orthogonal components of the magnetic anomaly vector.

This study adopts Pilkington's inversion of normalized source strength (NSS) and magnetic anomaly amplitude. Inversion of NSS derived from magnetic gradient tensor, was developed by Pilkington and Beiki (2013) and this scrutinizes the eigen value decomposition of magnetic gradient tensor as shown in equation 7;

$$T = \nabla\vec{B}_a^T = RAR^T \quad (7)$$

Where $T = \nabla\vec{B}_a^T$ = magnetic gradient Tensor;

R = orthonormal eigenvector matrix; A = eigen vector matrix with eigen values in descending order $\lambda_1 > \lambda_2 > \lambda_3$= diagonal elements and the tensor invariant quantity μ is defined as:

$$\mu = \sqrt{-\lambda_2^2 - \lambda_1\lambda_3} \quad \text{(Wilson, 1985)} \quad (8)$$

Where μ = tensor invariant quantity and it is directly proportional to dipole moment and independent of orientation as shown in equation 9;

$$\mu = \frac{\mu_{0_3} |\vec{m}|}{4\pi |\vec{r} - \vec{r}_3|^4} \quad (9)$$

where $|\vec{m}|$ = dipole moment, $\vec{r}_0$ & $\vec{r}$ = source and observed location respectively.

The NSS is independent of direction for dipole and spherical source cases (Schmidt *et al*., 2004). It does not affect random 3D sources, hence its use in 3D interpretation of magnetic data (Beiki *et al*., 2012 and Clark, 2013). NSS requires the conversion of total field anomaly to three orthogonal components; B_{ax} B_{ay} *and* B_{az} and computation of derivatives to create gradient tensors in order to have a better performance of the NSS inversion. At each location on the magnetic anomaly map, eigen value decomposition is applied to computed gradient tensor which makes the NSS operation complex and the measured gradient tensor can be directly used in the decomposition. Amplification of noise in the derivative calculations during gradient computations was reduced to the barest minimum.

4.0 RESULTS AND DISCUSSION

4.1 Lineaments Distribution

Figure 3 shows Landsat derived lineament densities in the range of between 0.46 and 1.03. Dense concentrations of lineaments were observed in the northeastern, central, northwestern and southwestern parts of the study area and in parts of Enugu, Anambra, Imo, Abia, Akwa Ibom, Ebonyi and Cross River States (Figure 3). These surface and subsurface lineaments are manifestation of fractures and fissures, faults, intrusions, topographic features, straight valleys, continuous scarps, straight rock boundaries, stream channels and systematic offset of rivers, sudden tonal variations and alignment of vegetation.

Three prominent trends of linear features were established from the lineament map as represented on the rosette diagram (Fig. 4). The major trends are E-W and N-S while majority of the lineaments trend in the ENE-WSW direction where lots of echelon fractures indicative of younger and most recent geodynamic events lie. The less prominent but denser lineaments trend is in the WNW-ESE direction where older lineaments most likely dominate and in less pronounced form. The summary of the results of statistical analysis of the lineaments are contained in Figure 4. Linear features equal to or greater than 1 km in length are considered to have the greatest potential of being more fully developed and penetrating greater depths. (Opara *et al*., 2012). Lineaments with lengths < 1 km were automatically extracted from Figure 3 and reproduced in Figure 5 with dominant trends in the E-W, N-S, NE-SW, NNE-SSW and ENE-WSW directions. High density lineaments occur in the area around Okigwe, Afikpo, Okposi, Awgu, Awka, Udi, Nsukka and Ogoja. The dense lineaments around Calabar flank are created by intense tectonic activity along the Cross River channel. The establishment of the linear features in this area corroborates some of the findings of Cratchley and Jones (1965) who observed that the Cretaceous rocks were highly deformed with intrusive concealing rift structure directions. Major deformational structures such as the Abakaliki Anticlinorium and the Afikpo Syncline as observed by Murat (1972), display NE-SW trending faults. It also agrees with the findings of Umeji (1988) that the lower Cretaceous is characterized by NE-SW oriented shear zones and fractures controlled by volcanism. He also postulated that NNE-SSW and NNW-SSE trending shear zones and fractures characterize the PAN-African Shields as well. Benkhelil (1989) discovered that the compressional folding

during the mid-Santonian tectonic episode affected the whole of the Benue Trough and was quite intense, producing over 100 anticlines and synclines, which most likely would have caused the genesis of structures within the study area.

Lineaments were also extracted from magnetic data. The magnetic lineament map (Fig. 6) shows deep-seated sources than Landsat's surficial lineaments. Lineament trends range from E-W (dominant trend) to NW-SE, NE-SW and N-S

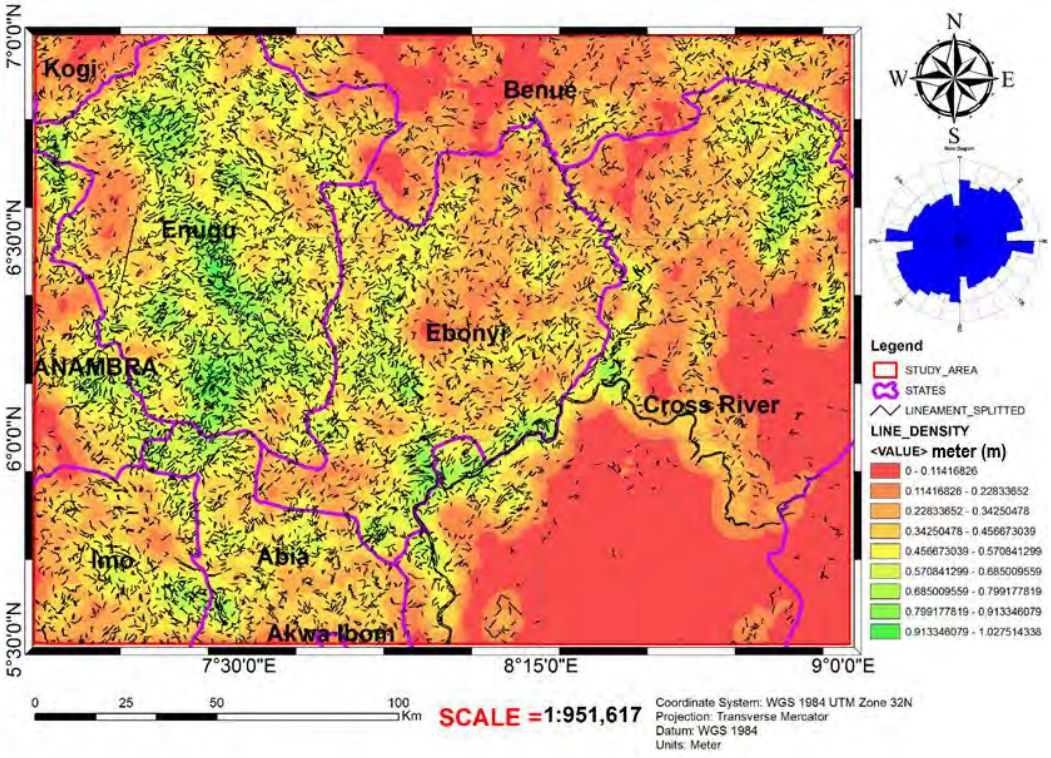


Figure 3: Landsat8 Lineament Density Map

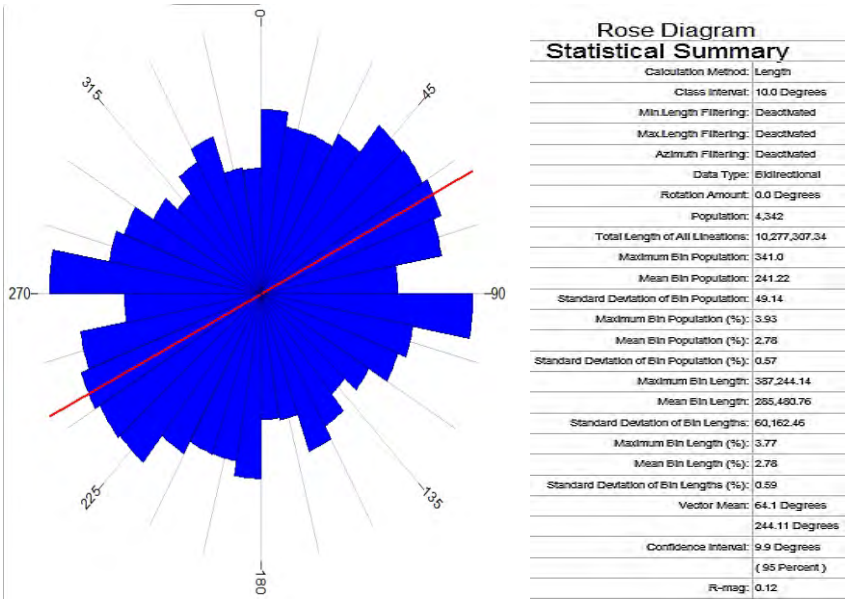


Figure 4: Rosette plot of the basicLandsat8 lineament trends

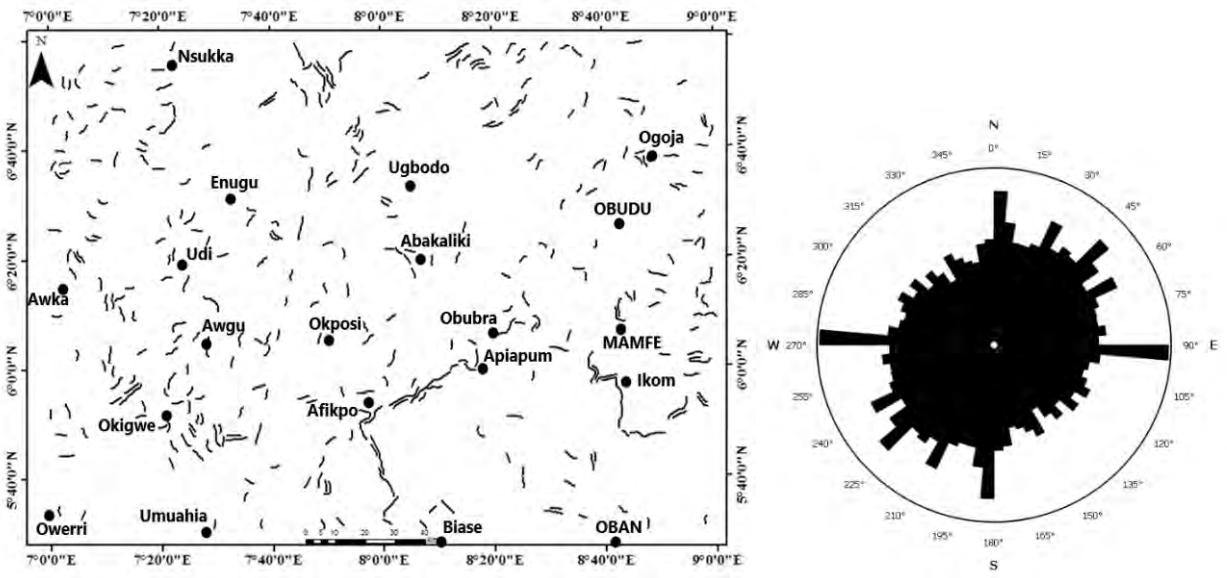


Figure 5: Automatically extracted Landsat lineaments and their trends

(Figure. 7). There are more surface lineaments in the ENE-WSW direction than the dominant E-W deep-seated lineaments around the study area.

4.2 Structures and Lithologic Alterations

Figure 8 shows the colour composite map which gives reflection of earth's surface material (aggregate of top 15 cm of the earth).

The 4/2 ratio composite map discriminates iron oxide rich rocks from host rocks. Iron oxide and hydroxide minerals such as hematite, jarosite and limonite have high reflectance within 0.63 to 0.69 µm which is equivalent to band 4 wavelength and high absorption within 0.45 to 0.52, equivalent to band 2 wavelength of Landsat 8. Iron oxide depicting ferrous content, comes out clearly in red colour band (Figure 9), evident from the high ratio value of 1.56501 which is >0.69 µm threshold. Areas north and northeast of Ebonyi State, southeast of Enugu State and North of Anambra State depict ferruginized regions. Ratio image of band 6 over band 7 (Figure 10) distinguishes altered rocks containing clays and alunite where pixels are bright red from unaltered rocks. The delineation of clay and carbonate minerals requires bands 6 and 7 attributed to high reflectance in the wavelength of 1.55 to 1.75 µm and high absorption in 2.08 to 2.35 µm. Areas coloured green up to red represent zones rich in clay minerals such as illite, kaolinite, and montmorillonite and the blue coloured parts are located over unaltered basement rocks of the Calabar flank. Band 6 over band 5 discriminates ferrous minerals in bright red tone (Figure 11) just like ratio 4 over 2 with high reflectance from 1.57 to 1.65 µm and high absorption from 0.85 to 0.88 µm wavelengths. The areas with bright red highlight regions rich in ferrous (magmatic) materials.

Sabin's ratio is used for mapping lithologies and hydrothermal alteration zones (sediment-hosted ore fields). This ratio composite is established in combination of 4/2, 6/7 and 6/5 as RGB respectively (Figure12). Light yellow to green colour represents hydrothermal alterations in outcropping formations while areas in blue represent dense vegetation. Possible hydrothermal alterations are highlighted in green by outcropping rocks. The ratio 6/7 was used to map clay minerals such as kaolinite, illite and

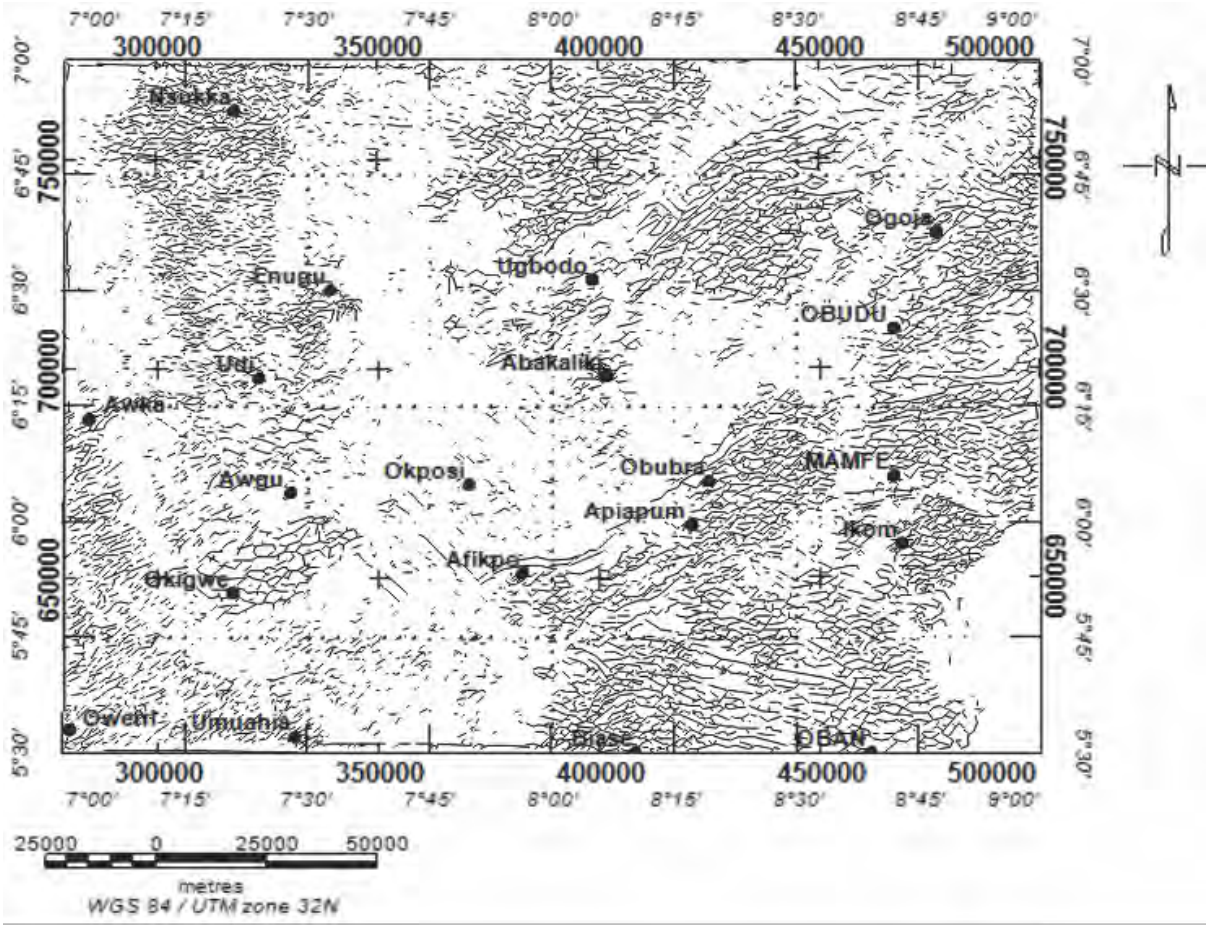


Figure 6: Lineament map extracted from magnetic data showing available trends in all directions

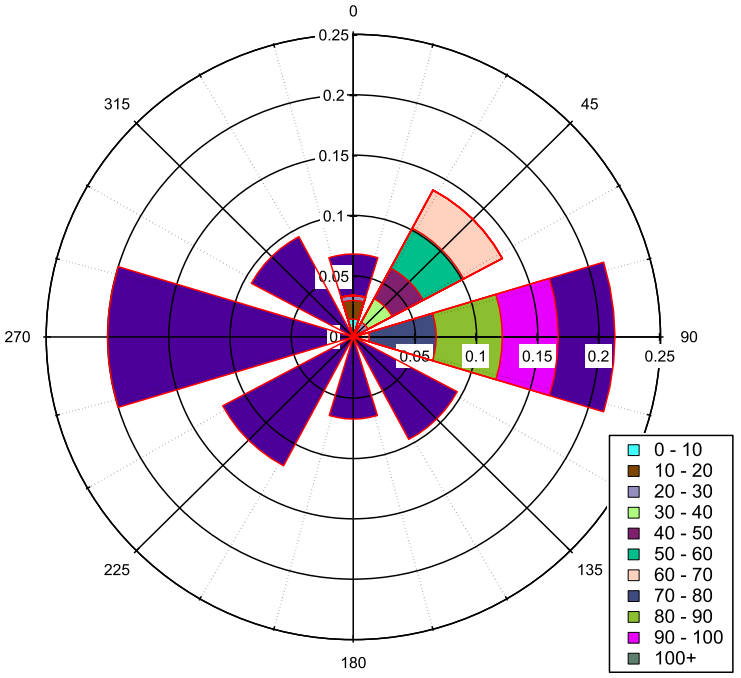


Figure 7: Strike component derived directly from the geomagnetic anomaly data

montmorillonite. The ratios 4/2 and 6/5 show high reflectance in the presence of ferrous minerals, thus these combinations detect suspected iron oxides rich ores such as hematite, limonite, jarosite hence their high reflectance in red region. The composites of Sabin's ratio highlight same areas of distinct alterations. Band 6 on 7 which delineates clay alteration regions was superimposed on the extracted magnetic lineament map (Figure 13) to show areas likely viable for ore accretions. The encircled zones are considered likely viable for ore formation because they are contact zones where lineaments directly coincide with areas in green and red denoting rich clay mineral regions.

These contact regions are believed to have resulted from the leaching properties of hydrothermal/ore fluids which have been actively circulated through dilated fractures and are possibly generated from heat of subsea magma chamber associated with upwelling magmatic plumes which intrude into sediments and are saturated by saline sea waters of high Sulpho-salts. Metals dissolved in sediments through seawater convection pass through sub-surfaces at varying depths before erupting to the surface, hence this constitutes the SedEx deposits linked to varying depths of occurrences of mineralizing fluids. Fluids penetrating shallow depths pick up Iron and Manganese, at deeper depths, pick up Lead and Zinc and at much greater depths, pick up Copper. The encircled zones in Figure 13 therefore approximates shallow to deeper accrued ores from mineralizing fluids in contact with these dilated fractures as revealed from magnetic lineaments.

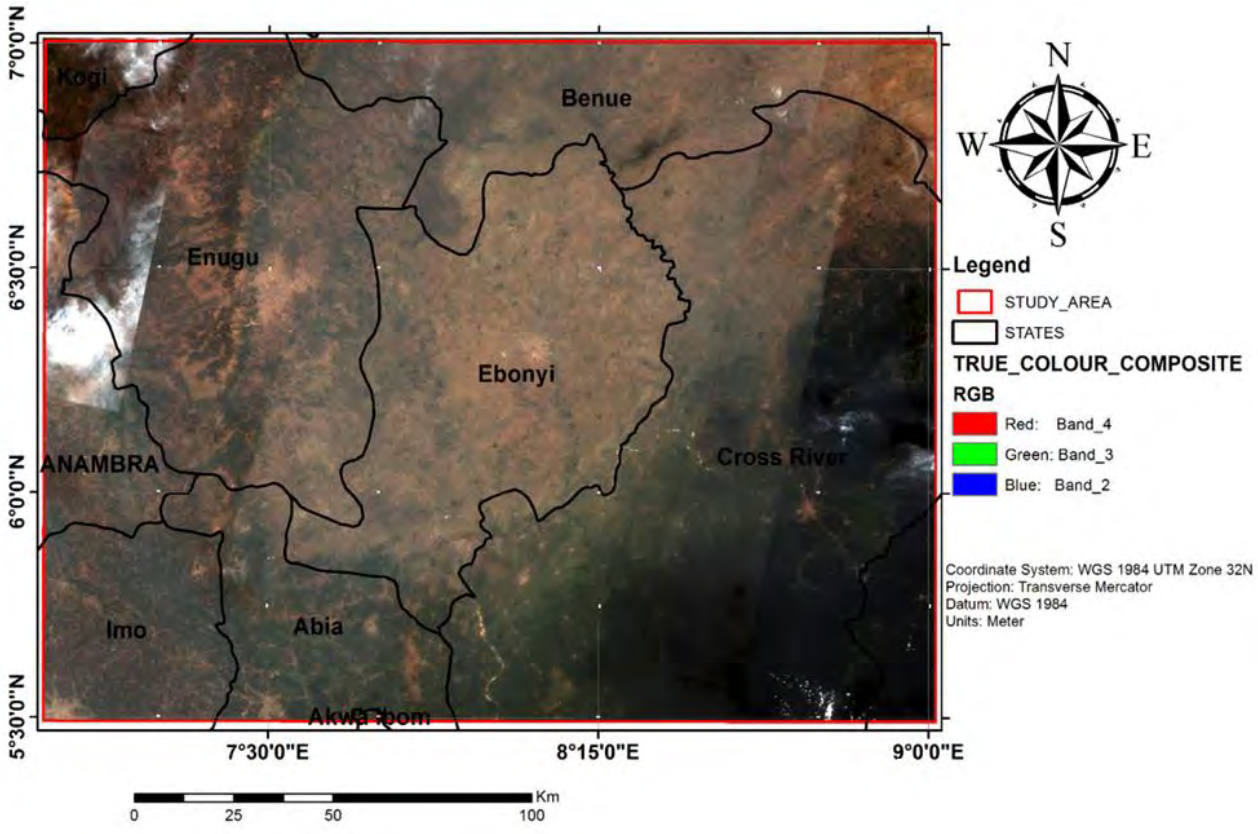


Figure 8: True Colour Composite Map

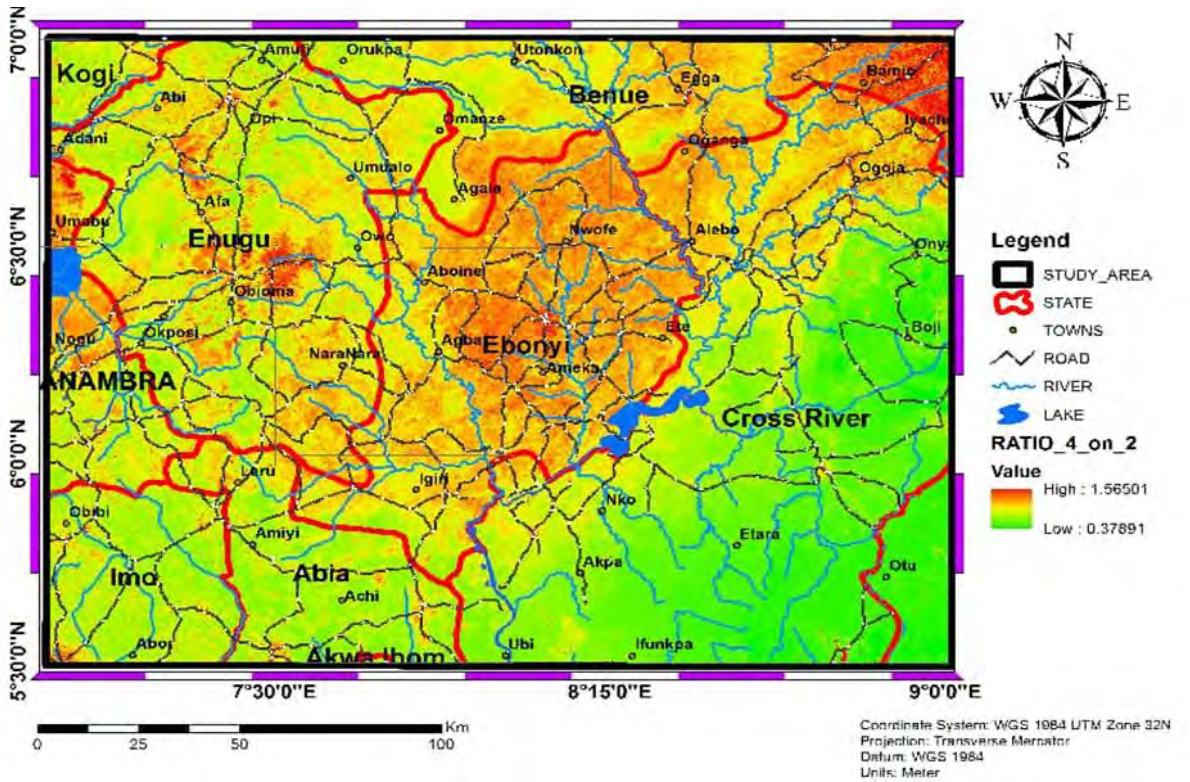


Figure 9: Ratio $\frac{4}{2}$ Iron Oxide Map

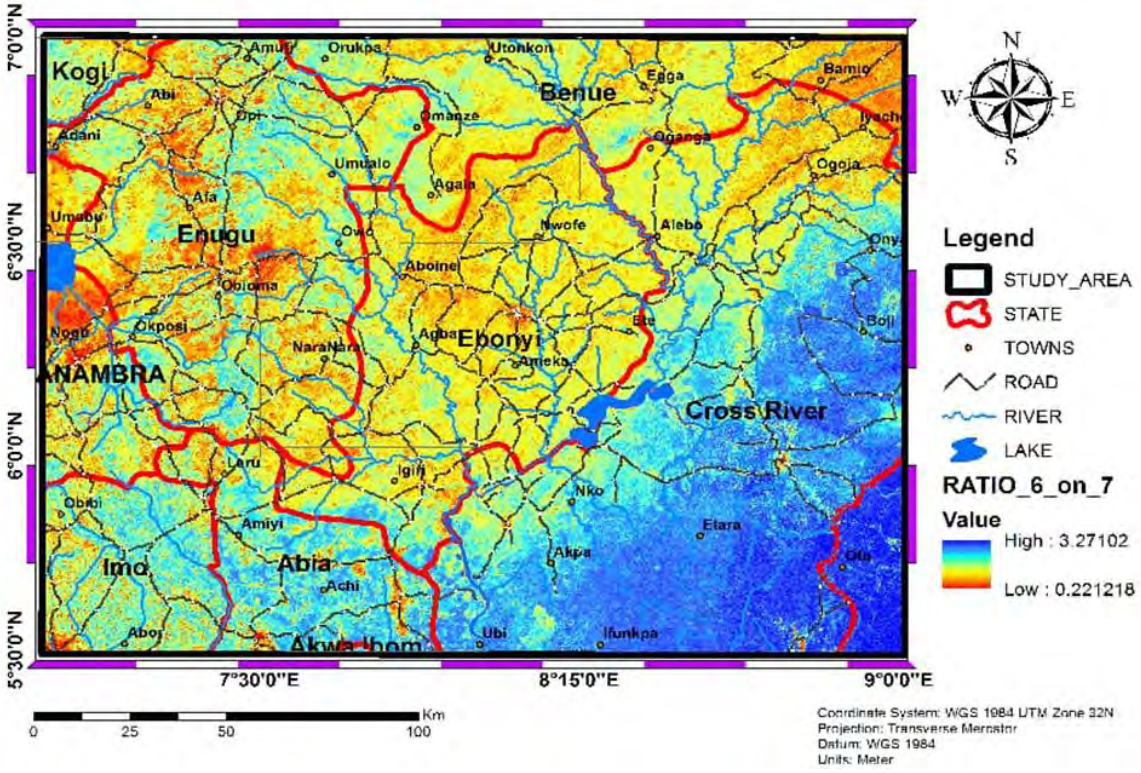


Figure 10: Ratio $\frac{6}{7}$ Clay Alteration Map

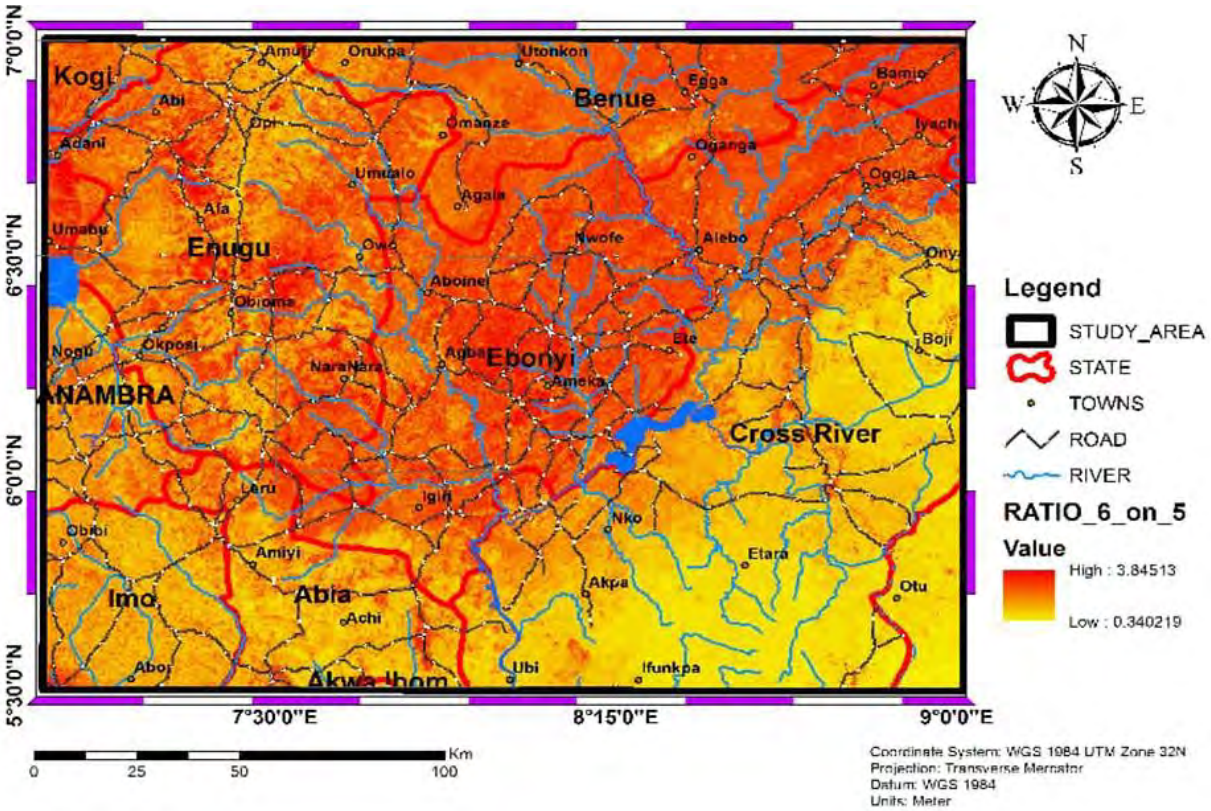


Figure 11: Ratio $\frac{6}{5}$ Ferrous mineral Map

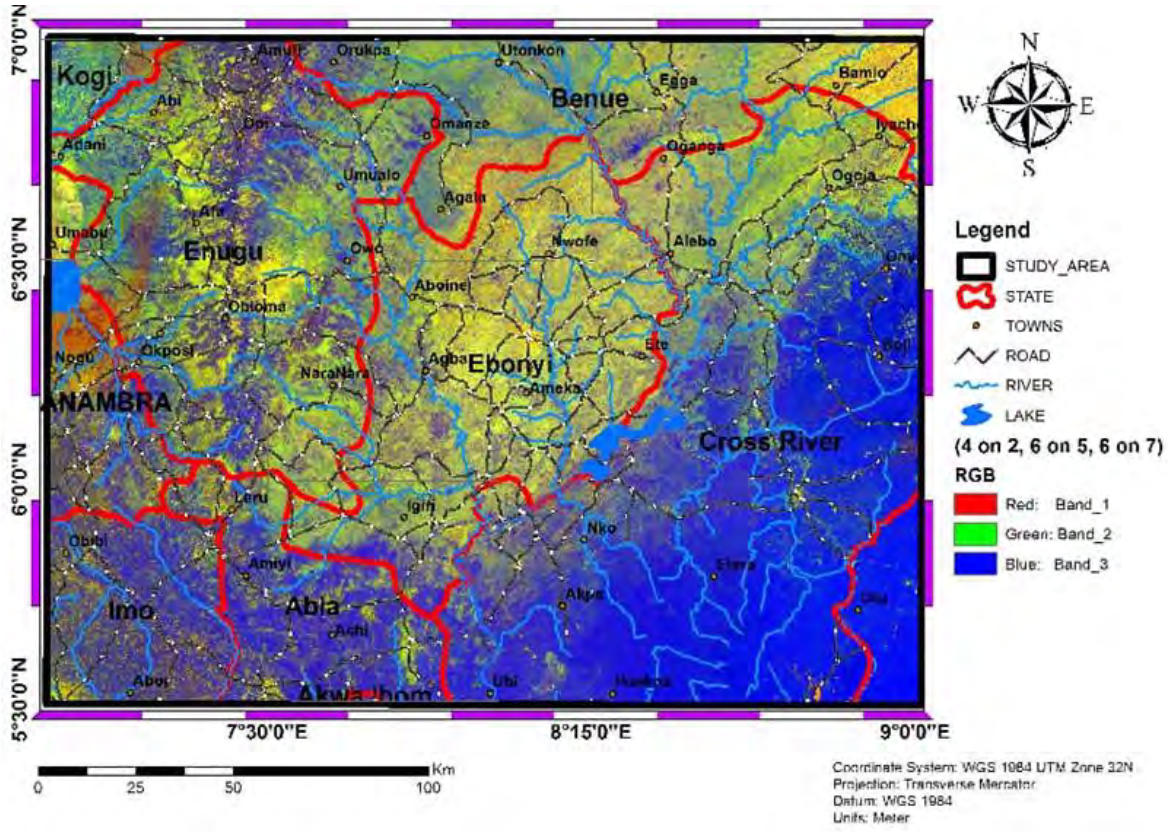


Figure 12: Ratio $\frac{4}{2}\frac{6}{5}\frac{6}{7}$ Ferrous mineral Map

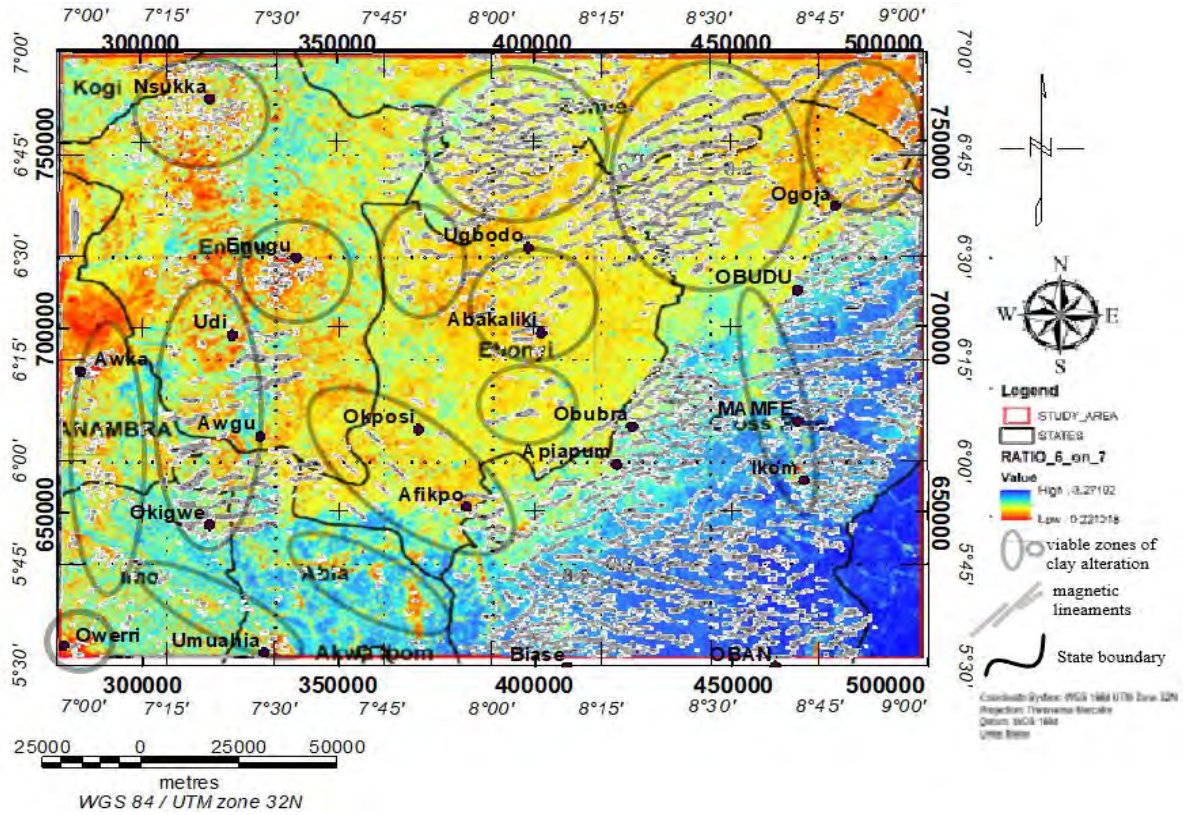


Figure 13: Magnetic Lineament Superposed on Clay Alteration (6 on 7 Ratio) Map

These zones, if further probed, have likelihood of sustainable Iron, Manganese, Lead and Zinc ore deposits in them. Magnetic and Landsat lineament maps were both superimposed on the iron oxide (4 on 2) map (Figures 14 and 15 respectively). The red iron rich zones which coincide with surface and deep seated lineaments are likely potential ore fields. The magnetic and landsat lineaments overlap significantly though the surface lineaments appear spatially distributed over the whole study area more than the magnetic lineaments. The superposition of extracted magnetic and Landsat lineaments show dense lineation which serve as good conduits to hydrothermal fluid migration, wall rock alteration and ore precipitation. Mineral map of the study area which was digitized from updated 2019 mineral map of Nigeria was superposed on the composite magnetic and Landsat lineament map (Figure 16). Areas with the occurrence of few existing minerals zones coincided with zones where surface and deep-seated lineaments co-occur, indicating likely fields where mineral deposits can be anticipated.

4.2.2. Interpretation of Aeromagnetic Data for Depth to Magnetic sources and Mineralization

The RTE-TMI map (Figure 17) reveals the magnetic basement as long wavelength anomalies, while the short wavelength anomalies are characteristic of shallow localized bodies, magnetic minerals/ore bodies and high magnetic intrusives. The map reveals high magnetic intensities in south-and northwestern parts of the study area. The lithologies and structures of the basement control the magnetic relief observed over the sedimentary basin.

The map displays isolated high magnetic anomalies typical of buried structures These

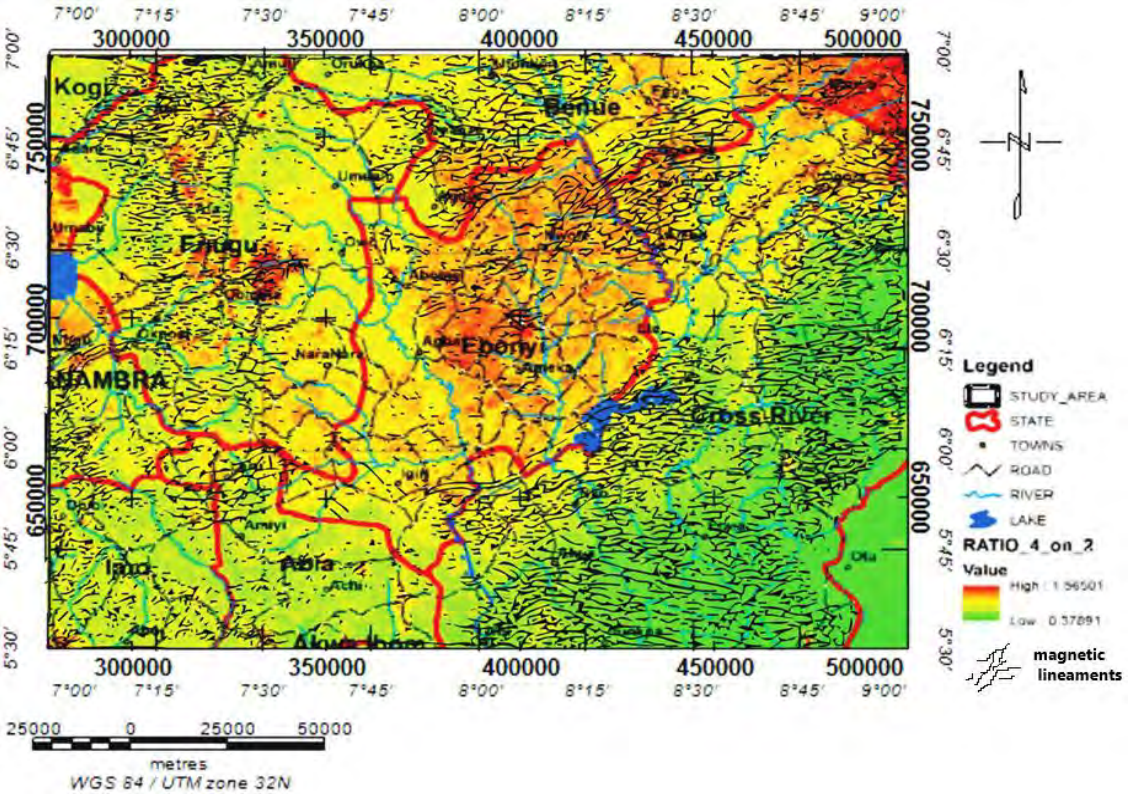


Figure 14: Magnetic lineament map on 4 on 2

anomalies are observed around Okigwe, Owerri, Okposi, Abakaliki, Enugu, Umuahia, Obubra and Apiapum. Corroborating this from Figure 13, areas with high magnetic responses coincide with encircled regions showing dual responses to clay alteration and dense magnetic lineations. Udensi and Akanbi and Udensi (2006) described elliptical or circular contours on magnetic anomaly maps as indicative of intrusions. These elliptically-shaped high magnetic anomalies which denote sub-surface intrusives relatively strike E-W and NE-SW as observed in Umuahia and Afikpo area. Areas with low magnetic relief on the RTE-TMI map include Ikom, Udi, Afikpo, Oban, Biase, Ogoja of the Calabar flank and Awgu. Owerri shows positive responses to both clay alterations and dense magnetic lineaments (Fig.13). The gullies and erosional activities around this area could have been initiated along fault zones. Reynold *et al*. (1990) and Opara (2011) also attributed a series of closed lows to depict linear trends which initiate shear/fault zones. Fault zones typify intrusive from basement which extend into sedimentary units and these contrasting lithological and tectonic units within the study area, precipitate varying magnetic responses (lows and highs). Around Ikom, North of Ugbodo and North-West of Ogoja, there seems to be responses from surficial localized bodies emanating from the basement because of adjacent low magnetic reliefs. These intrusives exist as veins which are embodiments of economic mineral aggregates as observed by Akpeke and Ekwueme, 2012, who showed typical barite bearing dolerite dykes, occupying the boundary between sandstone and basement. They also reported the occurrence of barite precipitation within calcareous sandstone and carbonaceous shale host rocks as a result of reaction of mineralizing fluids with calcareous sandstone, in Agoi Ibami, Cross River, State. The parent event of the Cretaceous African and South American

Continent rifting which initiated Albian Magmatic episodes and subsequent tectonic events from Santonian deformations produced dense lineaments with short and long wavelength responses on RTE-TMI map.

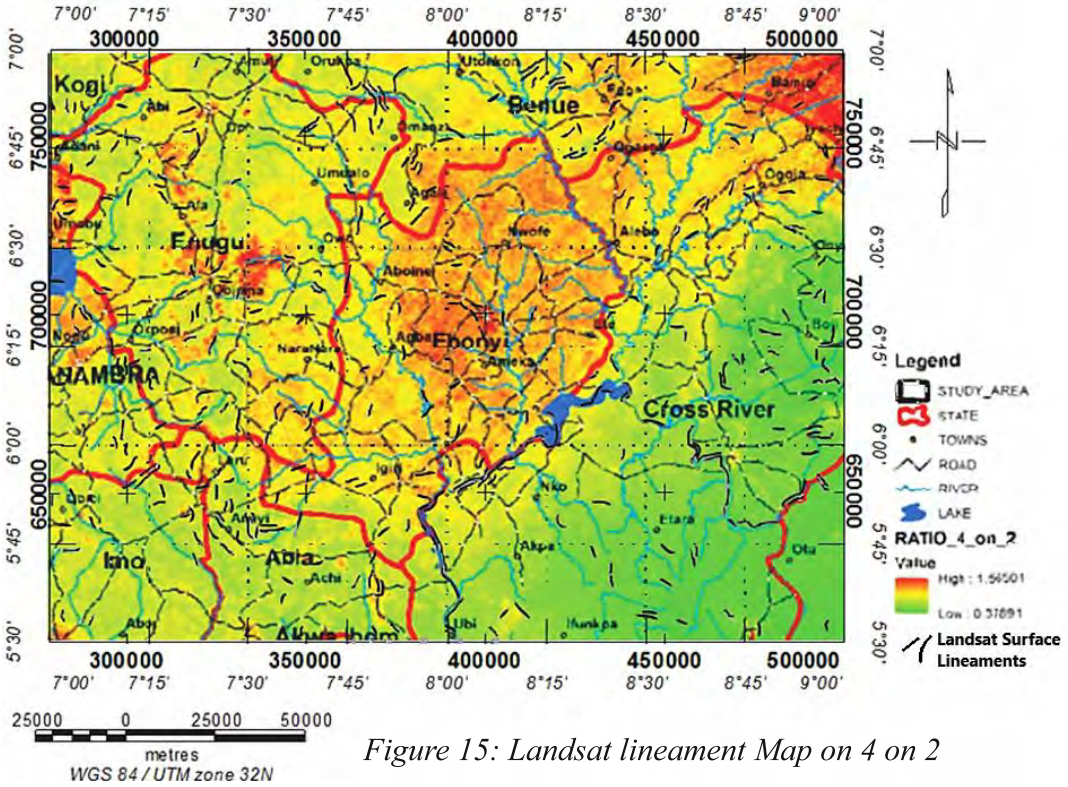


Figure 15: Landsat lineament Map on 4 on 2

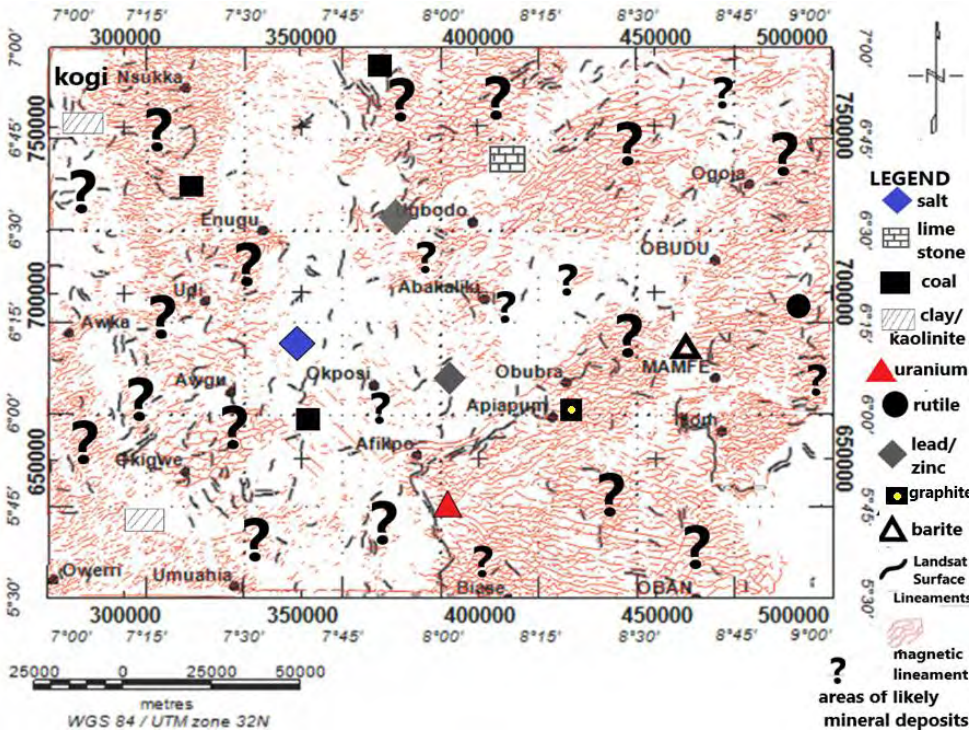


Figure 16: Superposed digitized mineral map (adapted from Falade,2016) on composite Landsat lineament and magnetic lineament map

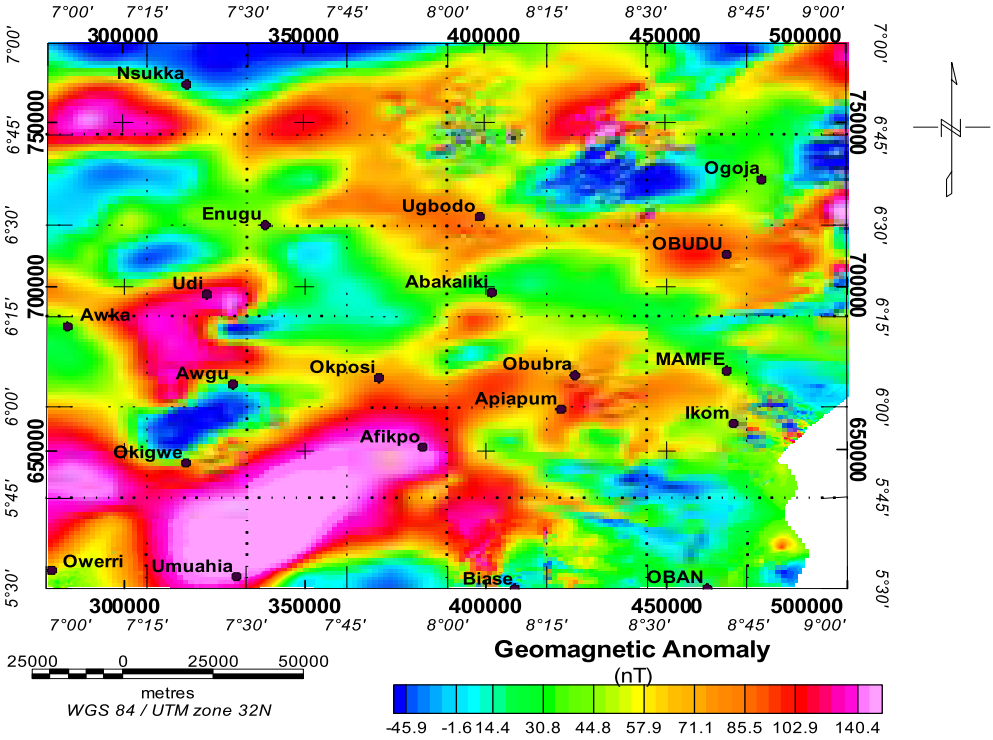


Figure 17: The RTE map of TMI Aeromagnetic Anomaly Map as obtained from NGSA

Edge Detection

The First Vertical Derivative (FVD) map (Figure 18) enhances the anomalies of shallow geological features. The variations in values depict lithological changes. Mafic rock-forming minerals and structural features in violet are revealed on the SVD map (Fig. 19). Shallow structural details of high magmatic origin as well as conspicuous but few magnetic lineaments (Fig. 18) with some of the magnetic lineaments display in Figure 6. The difference in magnetic mineral contents which manifests in various colourations on the SVD map, forms a major basis for lithological differentiation and delineation of boundaries. Opara *et al*. (2012) pointed out that high positive SVD values denote melanocratic rock forming minerals while low negative SVD values denote leucocratic rock forming minerals.

S observed by Oha *et al.* (2016), the SVD map reveals some major dispersions of shallow deposits demarcating lithologic outcrops. Zone denoted as A reveals subsurface outcrops of Oban Hill basement rocks, B, the mafics (basaltic/doleritic rocks) outcropping around Obubra, C, the mafics (basaltic rocks) around Ikom and D, the mafic to ultramafic rocks of the outcropping Obudu basement rocks. E_1 delineates pyroclastics of Abakaliki and other associated mafic rocks, E_2 have more surface magnetic responses from the Workum Hills and around Wanikande and Wanakom, E_3 represents near surface intrusives associated with barite mineralization around Gabu-Oshina. Some of the magmatic responses likely come from intrusive which are syn-depositional to ore deposits in a North-East trend. E_1, E_2 and E_3 in a dominant NE-SW structural trend fall categorically into parts of Abakaliki-Isiagu and Arufu- Akwana-Azara mineral district. Several concentrations of intrusive sills and dykes, bosses and stocks occur as lamprophyres, feldspathoidal syenite, leucodiorites, microdiorites gabbro and microgabbro are essentially posterior to the lead-

zinc mineralizations (Okezie, 1965). The ores of the Abakaliki-Isiagu deposits consist of massive sphalerite, galena, chalcopyrite, marcasite, siderite, calcite and quartz in descending abundance. Fluorite, quartz and minor galena disseminations are the mineral assemblages of the Arufu-Akwana-Azara mineral district. Sulfide minerals, such as sphalerite, galena and chalcopyrite are dominant in the Zurak-Wase deposits (Ogundipe and Obasi, 2016) district. F has lot of near surface intrusives characterizing Igumale, G represents responses from surficial Campanian-Maastrichtian-Paleocene carbonaceous shale and ferruginized ironstone capping overlying the sediments, H represents Okigwe-Ishiagu magmatic region still part of the Abakaliki-Ishiagu mineral district, This is part of the Albian Asu River Group facies which experienced two deformation (folding) phases (Nwachukwu, 1972; Amajor, 1985), offsetting magmatic activities, such as intrusion of dolerite and granitic dykes intrusions. Resultant hydrothermal ore mineralization like Pb-Zn mineralization arose as a result of this, and I represents responses from variegated ferruginized silts and sands of Nsukka formation in upper Anambra Basin with parts of this formation occurring in lower parts of Niger Delta formation.

Source Depth Estimation and Modelling of Structures

Two methods were adopted for depth estimation which include Magnetic Vector Inversion modeling (MVI) and 3D Euler De-convolution of the aeromagnetic data. Ten anomaly windows were captured on the geomagnetic anomaly map for more detailed probe using the Magnetic Vector Inversion modeling. These windows are labelled from P – Y as represented in Figure 20. The prominent anomalies which fall within these windows coincide with zones of clay alteration on Figure 13.

Six (6) windows, P,Q,S,U,V and Y, were chosen for discussion of inversion modeling results. The models delineated within window P occur at depths of between 2 and 7 km are shown in Figure 21. At the extreme northeastern part, where Nsukka is located, the models outcropping almost very close to the surface. Between 500 m to 2 km are low magnetic models most likely of shale, clay or sand origin. Mirianrita *et al*. (2015) corroborate this through their findings that depths of 1644 to 3082.7 m showed sufficiently thick sediments suitable for hydrocarbon accumulation. South of this has adjacent occurrences of deposits with varying magnetic intensities between 2 km to 7 km depths.

Low magnetic anomaly at the northeastern part of the window area are responses from near-surface and low magnetic models while higher magnetic anomalies (Fig. 20) are responses from deposits located at depths >7 km BSL and with higher MVI values.

The Q window captures northwest of Ogoja and northeast of Ugbodo. Spaced, nucleated deposits and varying shapes of models which are steep, inclined and curved were delineated (Figure 22). At the extreme left, is a conspicuous and an almost spherical shaped deposit and variegated magnetic vector inversion values from the model yield which correspond to mixed magnetic anomaly responses from the aeromagnetic anomaly (Fig. 22). The vertically inclined models with varying magnetic intensities at the central part of the window directly have mixed magnetic responses, basically very low and a bit of higher magnetic anomaly responses. These models with higher magnetic intensities at depth in the northwestern part of the window have higher magnetic anomaly responses. The deposits occur at varying depths of about 50m asl to >7km bsl.

The S window, captures Udi and Enugu area. In this area, horizontal models with varying MVI values were delineated (Figure 23). Horizontal

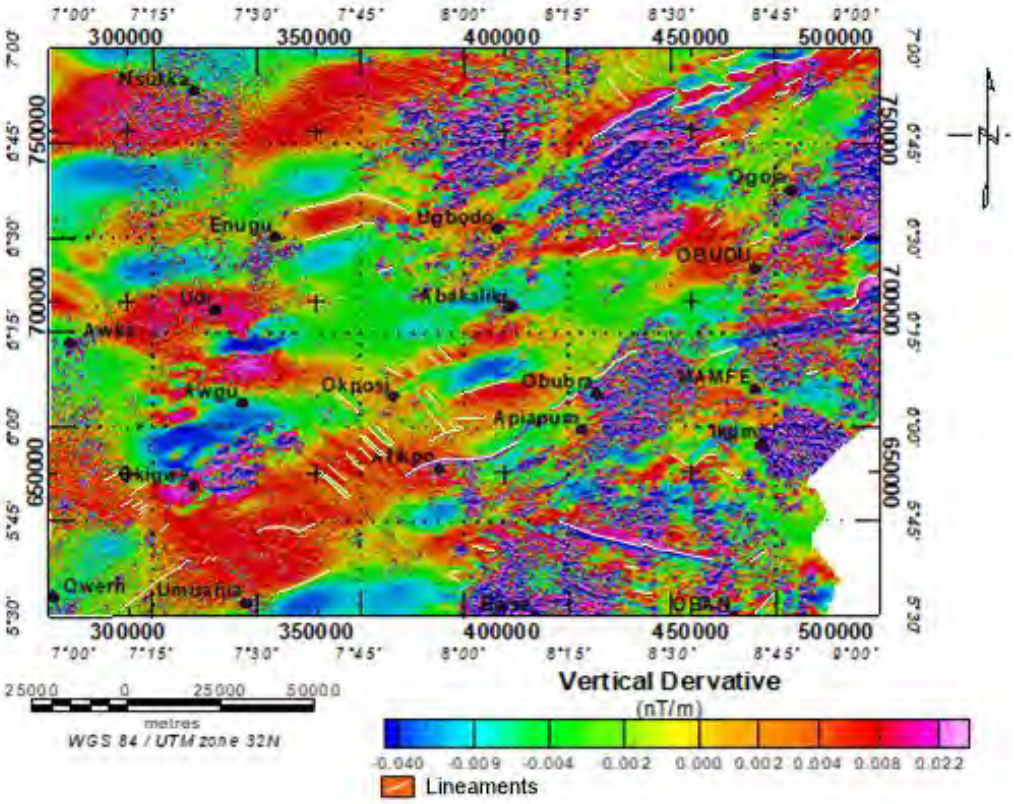
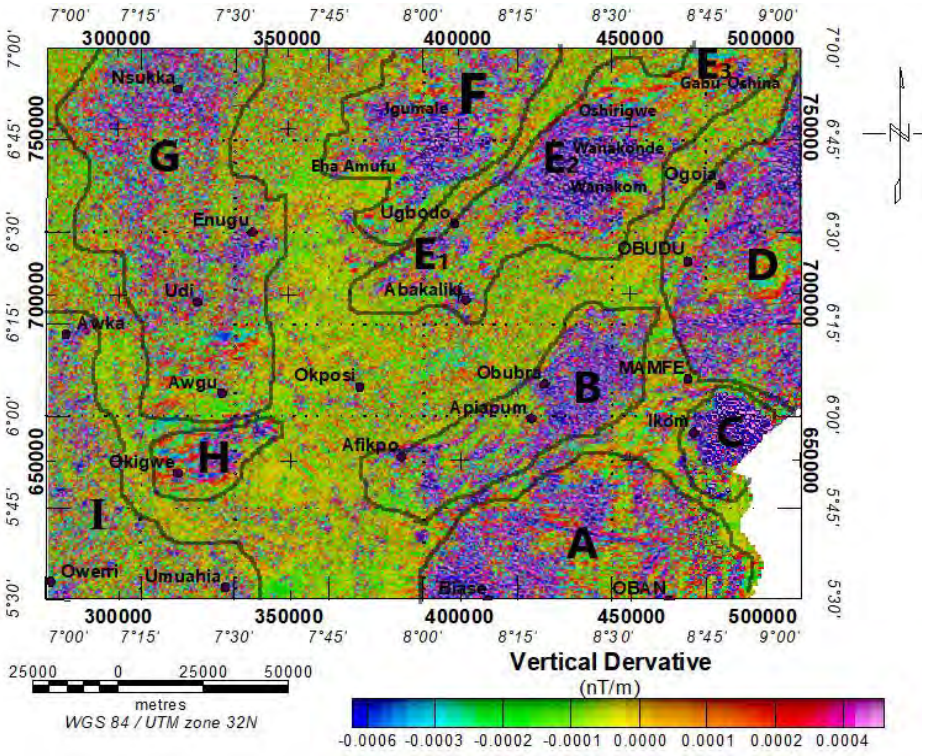


Figure 18. First Vertical Derivative Map with Superimposed Lineaments


Nsukka
Igumale
Eha Amufu
Enugu
Ugbodo
Oshirigwe
Wanakonde
Wanakom
Ogoja
OBUDU
Udi
Abakaliki
Awka
Awgu
Okposi
Obubra
MAMFE
Apiapum
Ikom
Afikpo
Okigwe
Owerri
Umuahia
Bende
Ohafia
Abia
Gabu-Oshina
Ohafia
Bende
Abia
Ikwuano
Umuahia
Isiala Ngwa
Aba
Owerri
Orlu
Oguta
Ohaji/Egbema
Mbaitoli
Ikeduru
Mbaitoli
Ikeduru
Mbaitoli
Ikeduru
Isiala Mbano
Mbaitoli
Ikeduru
Isiala Mbano
Mbaitoli
Ikeduru
Isiala Mbano

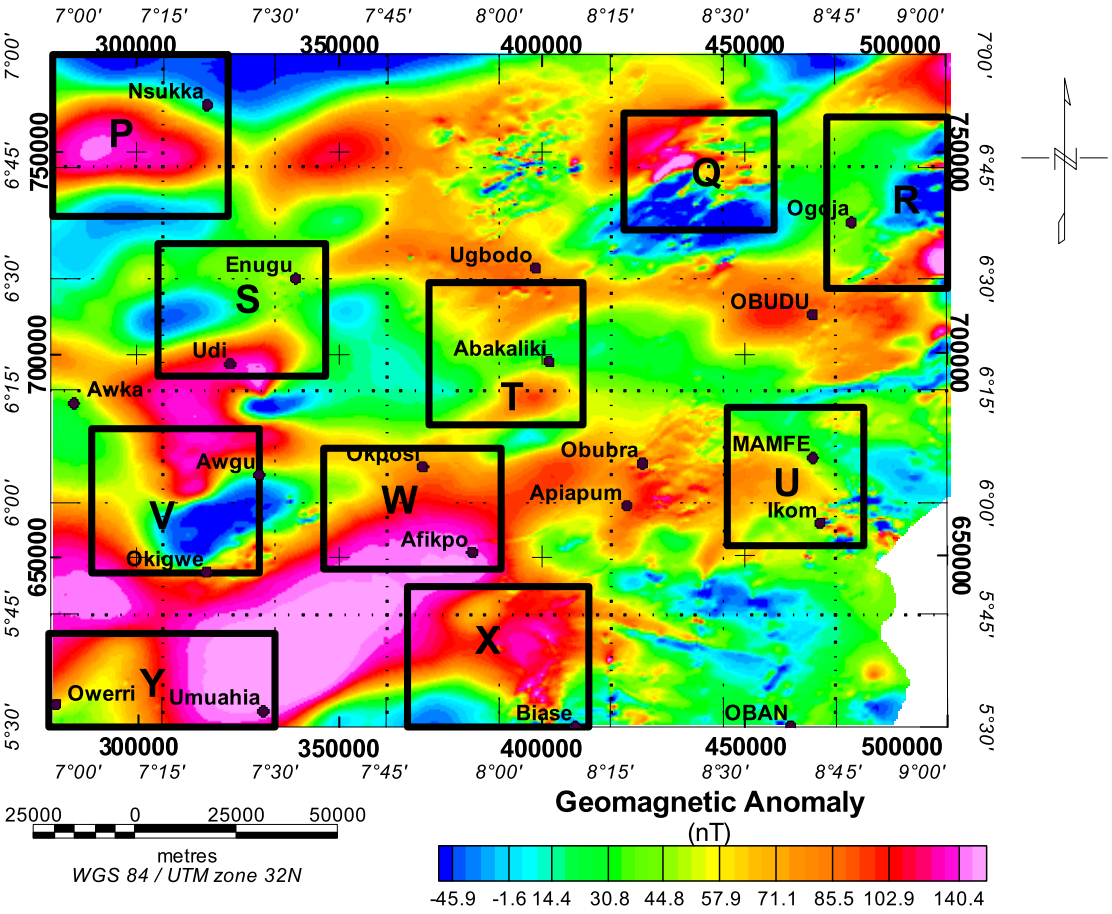


Figure 20. Pominent anomaly windows captured on the RTE-TMI Map

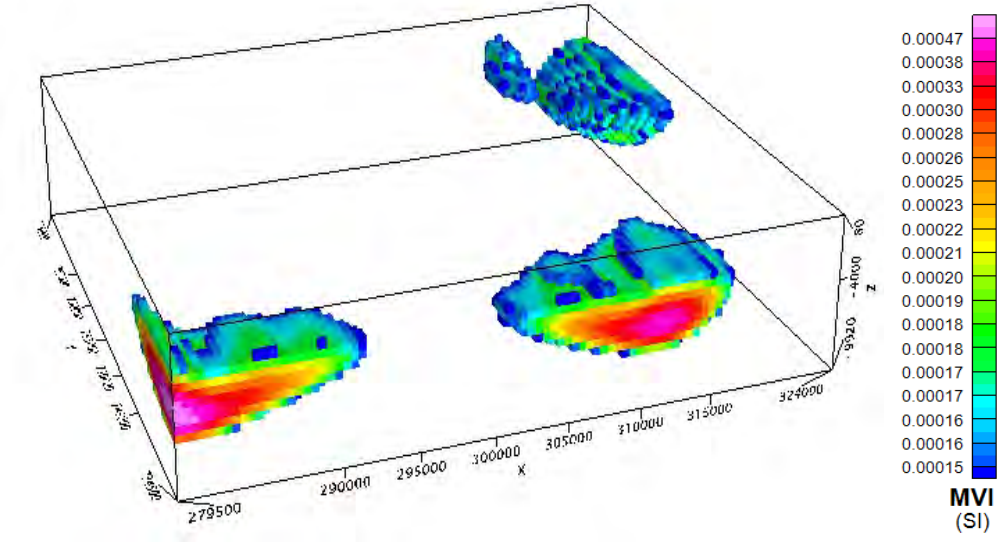


Figure 21: Inversion modeling results from window P

cylindrical dykes >30 km in length and trending N-S were mostly delineated at about >7 km bsl. At the eastern section of this window, sub-surface horizontal models became more reduced in length, occurring at about 500 m and up to more than 4 km. Over the rows of horizontal deposits with varying MVI values occurring at depths, are corresponding high magnetic intensity anomalies (Figure 20).

Window U captures the area around Ikom and Mamfe Basin of the Calabar flank. The model delineated around Ikom with varying range of MVI values, outcrops at the surface and extends to

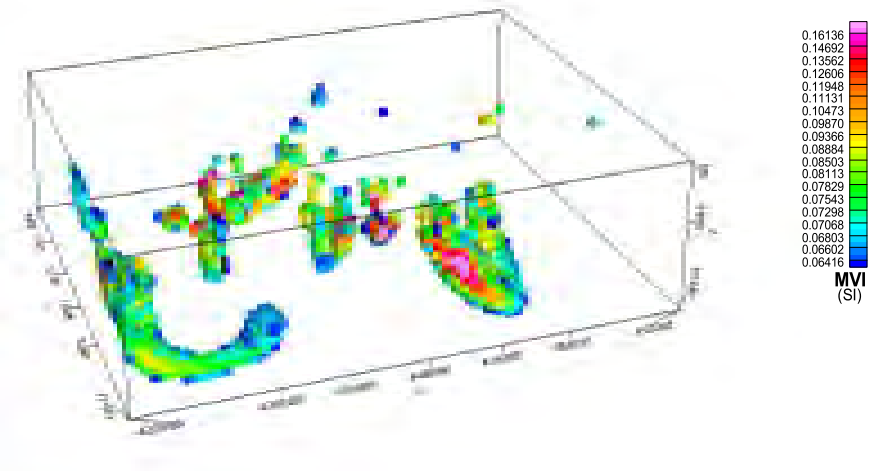


Figure 22: Inversion modelling results from window Q

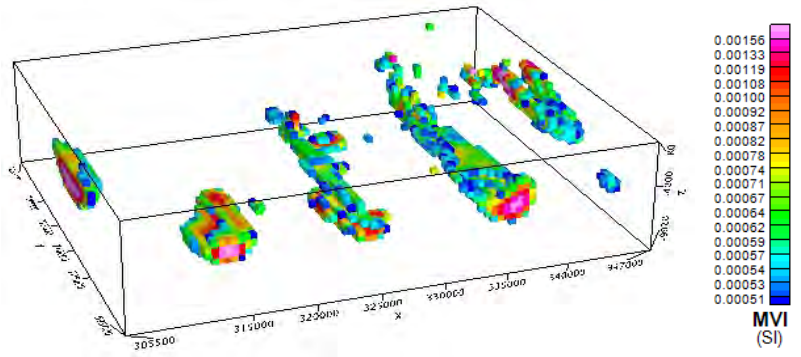


Figure 23: Inversion modeling results from window S

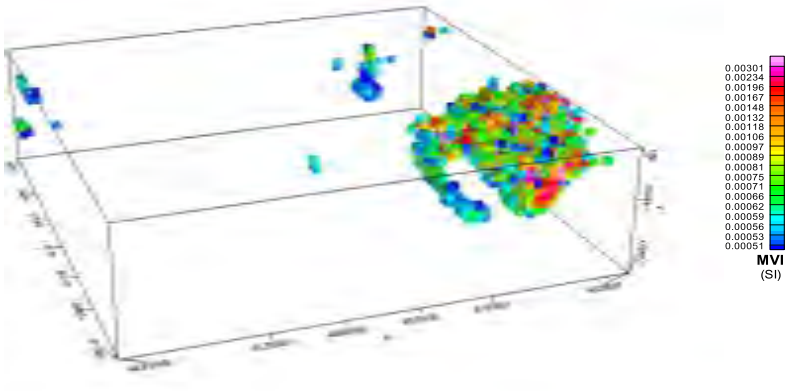


Figure 24: Inversion modeling results from window U

as much as >300 m asl as seen at the extreme right of the window and occurring also at depth of <6 km bsl (Figure 24). The variegated short wavelength anomalies correspond with the underlying model while high magnetic anomalies correspond with near-surface models (Figure 20).

Window Y captures the area around Owerri and Umuahia (Figure 25). Sub-surface structures are revealed within this window which occur at depths <100 m asl to as much as <5 km bsl. The deposits are almost spherical to nodular and dispersed as disseminated in-fillings all through the window area with MVI values in the range 0.00048 to 0.00069. Figure 20 shows a high anomaly response over the deposits at the extreme right of the window. From every window taken, deposits at varying depths were delineated. Most of the structures occur at between 100 m asl to up to > 7 km bsl.

The structural indices of 3D Euler Deconvolution of 0, 1, and 2 were adopted in this study because of the suspicion that a wide range of geologic models present within the study area.

However, best solution clusters for contacts with maximum depth range of >2444.2 m were obtained with the index of 0. The Euler solutions show dense cluster solutions which reveal various geologic structures such as faults/fractures and geologic boundaries in dominant E-W and NE-SW subordinate trends (Figure 26a). The lineaments in the NE-SW trend are seen around places like Okigwe, Enugu, Ikom, Mamfe, Afikpo, Abakaliki, Biase alongside a shallow to moderate depth ring-like structure encircled in white at Mamfe. The Euler solution clusters were superposed on RTE-TMI map is presented as Figure 26b. The white circles on the map delineate short wavelength anomaly responses corresponding to shallow-average depth contacts of 700-800 m relative to other structures occurring at deeper depths. Likely occurrence of shallow deposits is most expected here. The 3D Euler Deconvolution technique reveals information on respective depths of occurrence of these afore-mentioned structures. However, both the finite and infinite source contacts have been identified from good clustering of Euler solutions at various locations on the map. These contacts revealed are most likely geologic contacts in form of fractures and faults with varying depth ranges of between <713 m and >2444 m. Almost all over the study area, these contacts and structures have occurrences at above 2 km depth as seen dominantly around Afikpo, Okposi, Oban, Ogoja and Abakaliki. This corroborates potential mineralized zones highlighted in Figures 13, 20 and 21. Some structures of high magnetic anomalies occur at shallow depths as low as 0.5 to 1.5 km as seen in the north and northeastern parts of the study area.

Awgu most likely has thinly bedded faults with spherical to cylindrical deposits (Figure 27) from MVI modelling of window V. This window captures the area around Okigwe and Awgu and shows an inclined structure dipping in a NW-SE direction attached to an almost spherical model. This inclined steep model of very low MVI values of between 0.00031 and 0.00032 outcrops as much as >80 m asl. The near-spherical model has a range of MVI values of between 0.00034 and 0.00049 and occurs between depths of >1.5 km to < 7 km. Shallow and deeper magnetic source bodies at 0.641 km and 3.088 km respectively have been proven to exist in Okigwe-Udi area (Onyewuchi and Ugwu, 2016). Low magnetic anomaly characterizes the spherical and inclined steep models with low MVI values (Figure 20).

5.0 CONCLUSIONS

Over 1000 lineaments were extracted from both true colour composite of the Landsat image and the further processed RTE-TMI map. These dense composite lineaments reveal both surface and

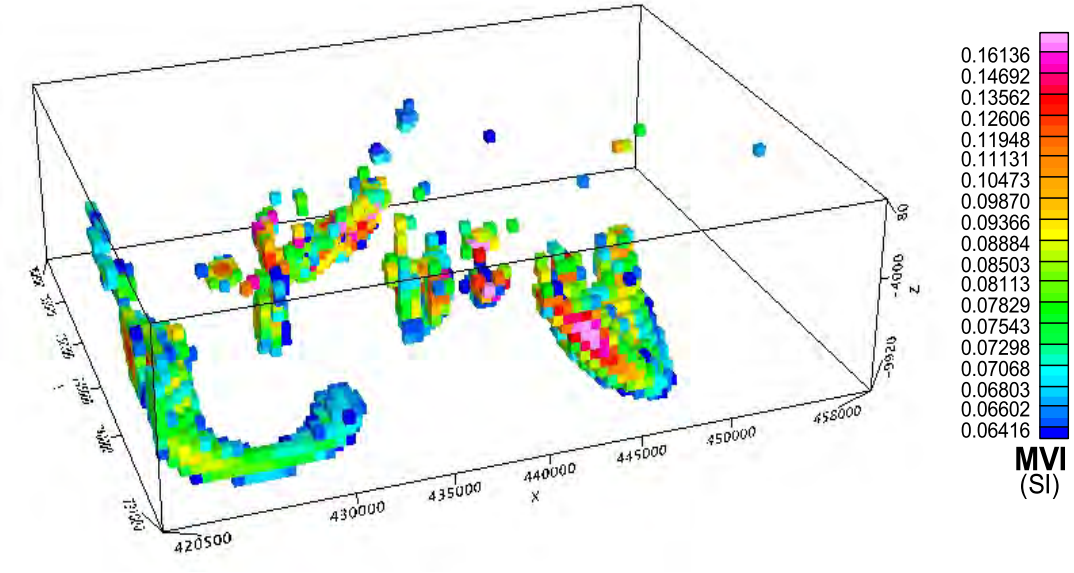


Figure 25: Inversion modeling results from window Y

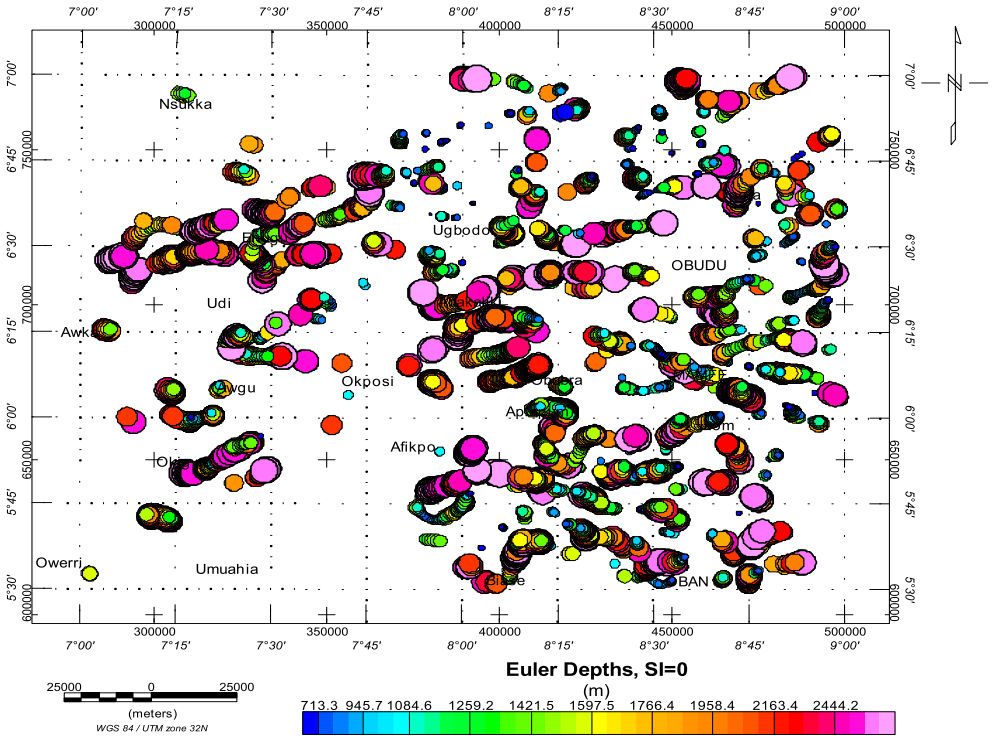


Figure 26a: Euler solution clusters for structural index (SI) = 0.

deep seated structures. The Nigerian southeastern sedimentary basin of the LBT reveals that about 70% of the area is covered by surface and deep-seated lineaments at depths >2km. About 50% of the basin contains shallow magmatic deposits in developed host rock lineaments to the range of 50-500 m and deep-seated ones occur at mostly >3km depths. These deposits have been modeled for their respective geometries which inform that most shallow deposits exist as spherical models, sills, inclined and horizontal cylindrical dykes. Magnetic lineaments with a predominant NE–SW

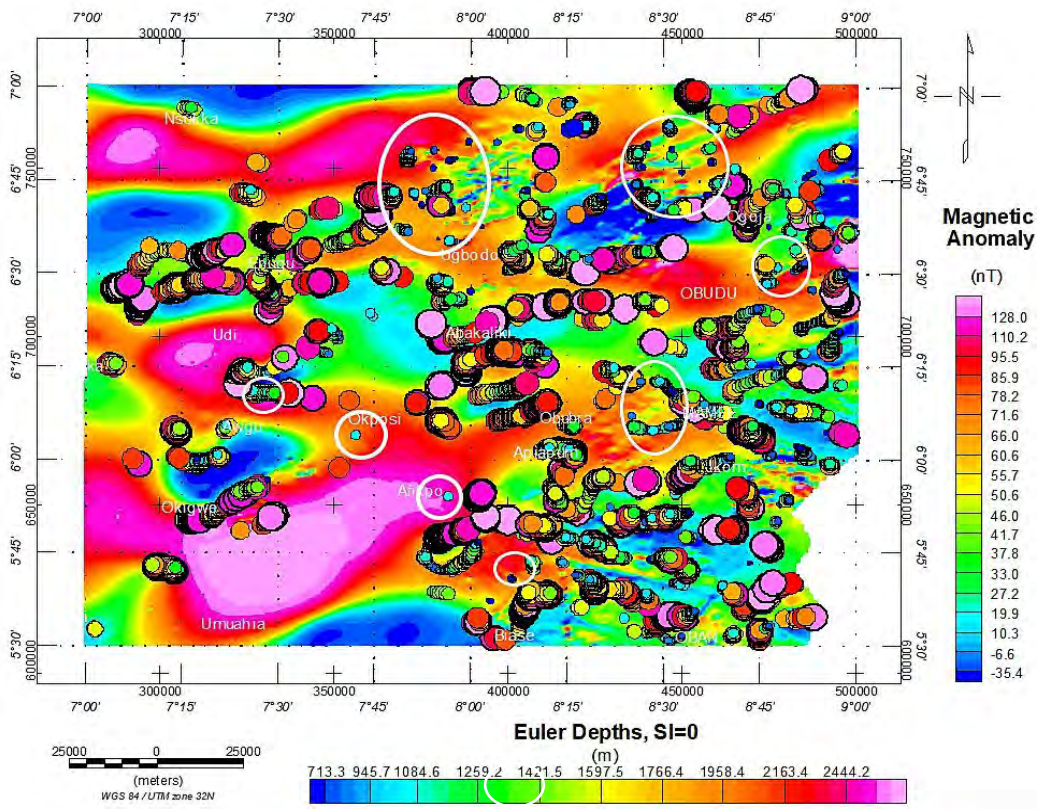


Figure 26b: 3D Euler depths solutions superposed on RTE-TMI map

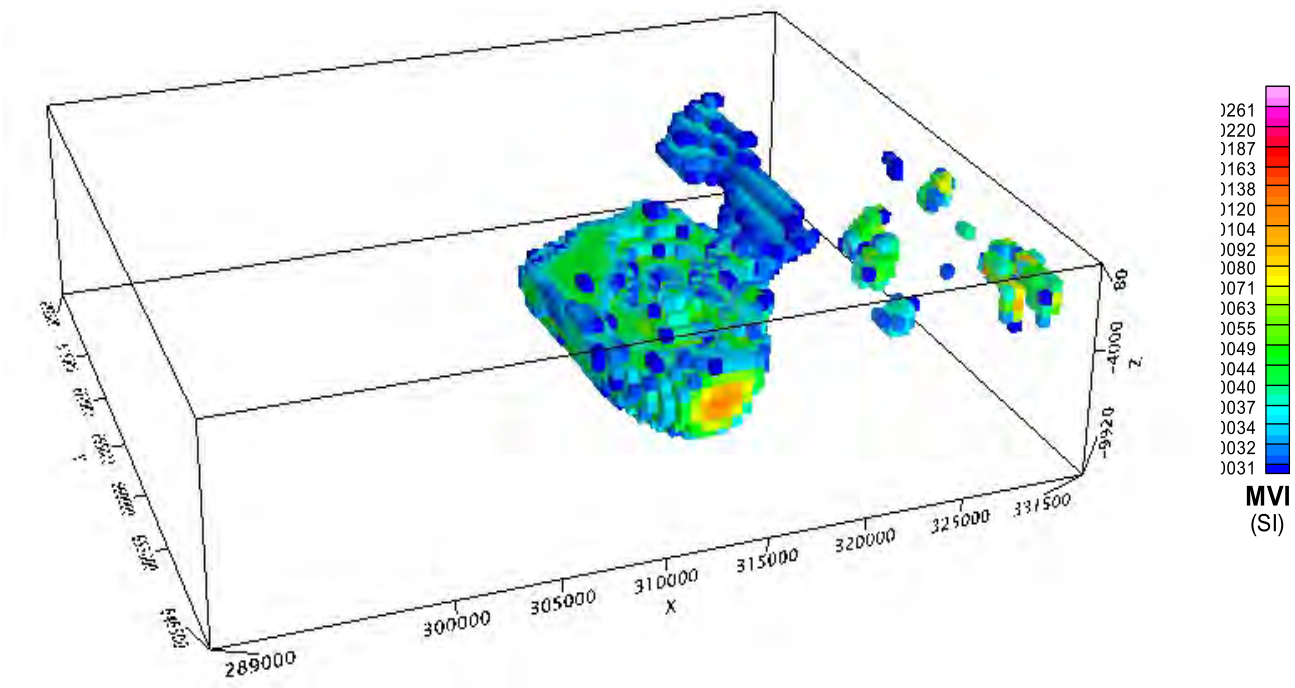


Figure 27: Inversion modeling results from window V capturing Awgu environs

trend appear to be more densely distributed around the basement rocks of the Oban Hills and metamorphosed rocks around the Workum Hills.

Magnetic lineaments have a predominant E-W trend while Landsat lineaments a dominant NE-SW trend. Few suspected mineral occurrences are situated mainly at regions where these lineament types co-occur. Sabin's ratio composites delineate alteration zones in the basin. The 3D Euler and MVI depth estimation techniques revealed dispersed occurrence of magnetic bodies at shallow depths of about 80-300 m, at moderate depths of about 400-1.5 km and at greater depth beyond 8 km.

The study concluded that the presence of dense lineaments from deformational events and intrusive amidst high temperature gradient generated from the Cretaceous magmatism makes the study area a potential ore field.

REFERENCES

Abdulrahman, A. K. (2010). Remote sensing. Republic of Iraq , Ministry of Higher Education and Scientific Research University of Technology, Department of Applied Sciences, University of Technology. Third Class, 1st Edition. Pp.15-17.

Abuzied, S. M. and Alreface, H. A. (2017). Mapping groundwater prospective zone integrating remote sensing, geographic information systems and geophysical techniques in El-Qaa Plain area Egypt, *Hydrogeology Journal*, vol.25, pp.2067-pp.2088. Springer-Verlag Berlin Heidelberg.

Adagunodo, T. A.; Sunmonu, L. A. and Adeniji, A. A.(2015). An overview of magnetic method in mineral exploration, *Journal of Global Ecology and Environment,* 3(1), pp. 13 - pp.28.

Aggarwal, S. (2004). Satellite remote sensing and GIS application in agricultural meterology. 23-28p. Geneva: World Meteorological Organization.

Akanbi, E-M and Udensi, E. E. (2006). Structural trends and spectral depth analysis of the residual field of Pategi Area, Nigeria, using aeromagnetic data, *Nigerian Journal of Physics,* 18(2), pp.271-pp.276.

Akande, S. O. and Mucke, A. (1993). Co-existing Copper Sulphides and Sulphosalts in the Abakaliki Pb–Zn deposit, Lower Benue Trough and their genetic *implications*, *Journal of Mineral. Petrology*., Vol.47, pp. 183–pp.192.

Akinlalu, A. A.; Adelusi, A. O.; Olayanju, G. M.; Adiat, K. A. N.; Omosuyi, G. O.; Anifowose, A. Y. B. and Akeredolu, B. E. (2018). Aeromagnetic mapping of basement structures and mineralization characteristics of Ilesa Schist Belt, Southwestern Nigeria, *Journal of African Earth Sciences*, Vol. 138, 383-391. DOI: https//doi.org/10.1016/j.jafrearsci.2017.11.033

Ali, A. and Amin, B. P. (2014). Lithologic mapping and *hydrothermal* alteration using Landsat 8 data. A case study in Ariab mining district, red sea hills, Sudan, *International journal of Sciences*(IJSBMR), 3(3), pp.199-pp.208. DOI.10.*14419*/ijbas.v3i3.2821.

Amajor, L. C.(1985). The Cenomanian hiatus in the Southern Benue Trough, Nigeria. Geological Magazines,122(01), pp.39-pp.50. Doi: 10.1017/s0016756800034063.

Ananaba, S. E. and Ajakaiye, D. E. (1987). Evidence of tectonic control of mineralization in Nigeria from lineament density analysis: A landsat study, International *Journal of Remote Sensing,* 8(10), pp.1445-pp.1453.

Anyanwu, G. and Mamah, L. (2013). Structural interpretation of Abakiliki-Ugep, using airborne magnetic and Landsat Thematic Mapper (TM)

Data, *Journal of Natural Sciences Research*, 3(13), pp.137-pp.149. ISSN 2224-3186(Paper), ISSN 2225-0921(Online).

Bamidele, O. E. (2020). Assessment of relationship between mineralization and structures within the Ijero mining field, southwestern Nigeria. *Unpublished* PhD *thesis*, Obafemi Awolowo university, Ile-Ife. Osun State, Nigeria. 463pp.

Beiki, M.; Clark, D. A.; Austin, J. R.; and Foss, C. (2012). Estimating source location using normalized magnetic source strength calculated from magnetic tensor data, *Geophysics Journal,* Vol.77, pp.23-pp.37.

Benkhelil, M. J. (1989). The origin and evolution of the Cretaceous Benue Trough, Nigeria, *Journal of Afrian. Earth Science*., Vol.8,pp. 251-pp.282.

Butler, K. (2013). ESRI band combinations, for Landsat 8 imagery and remote sensing. ARC GIS blog, ESRI USER conference.URL: http:www.nasa.gov/content/goddard/nasa-usgs-landsat-8-satellite-celebrates-first-year-of-success/#.UyIv1vl spo

Clark, D. A. (2013). New Approaches to dealing with remanence: magnetic moment analysis using tensor invariants and remote determination of insitu *magnetization* using a static tensor gradiometer (Extended Abstract) 7. 23rd International ASEG-PESA Geophysical Conference and Exhibition, Melbourne. (Chapter7), 11-14 August.

Cratchley, L. R. and Jones, C. P.(1965). An interpretation of the geology and gravity anomalies of the Benue Valley, Nigeria. Overseas geological surveys, Institute of Geol. Sciences, London, *Geophysics*, vol.1,pp.1-pp.26.

Dobrin, M. and Savit, C. (1988). Introduction to geophysical prospecting, McGraw Hill, 4th edn. ISBN-13:978-0070171961, ISBN-10:0070171963.

Doyle, H. A. (1990). Geophysical exploration for gold-A review. *Geophysics,* 55(2), pp.134-pp.146.

Drury, S. A. (1986). Remote sensing of geological structure *in* European agricultural terrain, *Geol. Mag.,* 123, pp.113-pp.121

Drury, S. A. (1993). Image interpretation in Geology. Second Edition, Allen and Unwin, London.

Egboka, B. C. and Uma, K. O. (1986). Hydrochemistry, contaminant transport and tectonic effects in the Uburu-Okposi salt lake area of Imo State, Nigeria. *Hydrologic, Scicence. Journal,* 31(2), pp205-pp.221.

Ekwueme, B. N. and Akpeke, G. B. (2012). Occurrence and distribution of barite mineralization in Cross River State, southeastern Nigeria, *Global Journal of Geological Sciences*, 10(1):pp.85-pp.98.

Encarta, Microsoft archived from *The Original.* (2009).

Etim, O. N.; Louis, P. and Maurin, J. C. (1988). Interpretation of electrical soundings on the Abakaliki Lead-Zinc and barite prospects, S.E. Nigeria: Geological and genetic implications, *Journal of African Earth Sciences,* Topographical map of the study area, Vol .7, pp.743-pp.747.

Evans, A. M. (Ed.) (1995). Introduction to mineral *exploration*. Blakwell Science Ltd., Paris, France.

Ezepue, M. C. (1984). The Geologic setting of Lead-Zinc deposits at Ishiagu, southeastern, Nigeria, *Journal of African Earth Sciences*, 2(2), pp.97-pp.101.

Falade, M. O. (2016). A profile of Nigeria's solid minerals. Overview of minerals in Nigeria. In:

Report of the Vision 2020, National Technical Working Group on MINERALS AND METALS DEVELOPMENT,2009.In:http://en.wikipedia.org/wiki/Mining_industry_ofNigeria. (Accessed October, 2018).

Farrington, J. L. (1952). A preliminary description of the *Nigerian* Lead-Zinc field, *Economic. Geol*., 47(6), pp.583-pp.608.

Fatoye, F. B and Gideon, Y. B. (2013). Geology and mineral resources of the Lower Benue Trough, Nigeria: Advances in Applied Science Research, *Pelagia Research Library*, 4(6):pp.21-pp.28. ISSN:0796-8610, CODEN (USA): *AASRFC*.

Fatoye, F. B.; Ibitomi, M. A. and Omada, J. I. (2014). Lead-Zinc-Barites mineralization in the Benue Trough, Nigeria: Their geology, occurrences and economic prospective. Advances in Applied Science Research, 5(2), pp.86-pp.92.

Fournier, D.; Heagy, L. J. and Oldenburg, D. W. (2020). Sparse magnetic vector inversion in spherical coordinates. *Geophysics,* Vol. 85, 33-J49. https://doi.org/10.1190/geo2019-0244.1. Oasis Montaj How-to-Guide. Magnetic lineament extraction, 3DEuler deconvolution, magnetic vector inversion. http://*geosoft*.com/

Glatzmaier, G. A. and Roberts, P. H. (1995). A three-dimensional self-consistent computer simulation of a geomagnetic field reversal, *Nature*, 377 (6546), pp.*203*-pp.209.

Goetz, A. F. H. and Rowan, L. C. (1981). Geologic remote sensing. *Science*, Vol. 211, pp.781-pp.791

Grant, F. K. (1971). South Atlantic, Benue Trough and Gulf of Guinea Cretaceous Triple Junction. *Geological Soc.iety American Bulletin,* Vol. 82, pp.2295-pp.2298.

Hoover, D. B.; Klein, D. P. and Campell, D. C. (1995). Geophysical methods in exploration and mineral environmental investigations. In: Edward, A. Ed.) Preliminary compilation of descriptive geoenvironmental mineral deposit models, *US Department of the Interior, US Geological Survey, Open-file Report*, 95-831, pp.19-pp.23.

Iloeje, N. P. (1981). A New Geography of Nigeria (New Revised Edition). Academy Press Ltd., Lagos, Nigeria.

Ilugbo, S. O. and Ozegin, K. O. (2018). Significance of deep seated lineament in groundwater studies around Ilesha, southwestern Nigeria. *Asian Journal of Geological Research,* 1(1), pp.1-pp.16.

Kolawole, M. S, Ameh, E. G. and Daniel, A. (2012). Preliminary lineament analysis within the vicinity of Kainji Dam, Nigeria, using ERS-1 SAR image. *Confluence Journal of Environmental Studies*, Vol.7, pp.95 – pp.102.

Leilesand, T. M and Keifer, R. (1993) Remote sensing and *image* imterpretation, third edition, pp.159. John Villey, New York, ISBN10:0471305758/ ISBN 13:9780471305750

Li, Y. (2017). From susceptibility to magnetization: *Advances* in the 3D inversion of magnetic data in the presence of significant remanent magnetization, paper, Vol.18, pp.239-pp.260.

Li, Y.; Shearer, S.; Haney, M. and Dannemillller (2010). Comprehensive approaches to the inversion magnetic data affected by remanent magnetization: *Geophysics*,Vol.75, pp.1-pp.11.

Liu, S.; Fedi, M.; Baniamerian, J. and Hu, X. (2017). Magnetization vector inversion of magnetic data and its application in mineral exploration of China. *GNGTS*, pp.704-pp.708.

Mirianrita, N.; Obiora, D. N.; Ossai and Okwoli, E. (2015). A case study of aeromagnetic data interpretation of Nsukka area, Enugu State, Nigeria, for hydrocarbon exploration. *International Journal of Physical Sciences, 1*0(17), pp.503-pp.519.

Murat, R. C. (1972). Stratigraphy and palaeography of the Cretaceous and Lower Tertiary in Southern Nigeria. *In: T.F.J Dessauvagie and A.J. Whiteman (Eds.),* African Geology, University of Ibadan, Nigeria, pp.251-pp.266.

Nabighian, M. N.; Grauch, V. J. S.; Hansen, R. O.; LaFehr, T. R.; Li, Y.; Pierce, J. W.; Philips, J. D. and Ruder, M.E. (2005). The historical development of the magnetic method in exploration. Geophysics, Vol.70, pp.83-pp.61.

Nash, C. R., Boshier, P. R., Coupard, M. M., Theron, A. C. and Wilson, T. G. (1980). Photogeology and satellite image interpretation in mineral exploration. *Mineral Science Eng*., vol.12, pp.216-pp.244.

Nigerian Geological Survey Agency (2010). Digitized map of the geology of Lower Sedimentary Basin from geologic map of Nigeria.

Nwachukwu, S. O. (1972). The tectonic evolution of the southern portion of the Benue Trough, *Geological. Magazine.* 109(5), pp. 411- pp.419.

Nwachukwu, S. O. (1974). Temperatures of formation of *vein* minerals in the southern portion of the Benue Trough, Nigeria. *J Mining Geol*., Vol. 11, pp.45- pp.54.

Obaje, N. G. (2009). Geology and mineral resources of Nigeria, pp.57-pp.60. Springer Dordrecht Heidelberg London New York, 2009. ISBN 9783540926849.

Obi, D. A.; Okereke C. S.; Obei B. C. and George A. M. (2009). Aeromagnetic modeling of subsurface intrusives and its implication on hydrocarbon evaluation of the Lower Benue Trough, Nigeria. *European Journal of Scientific Research*, 47(3), pp.347 – pp.361.

Odoma, A. N.; Obaje, N. G.; Omada, J. I.; Idakwo, S. O. and *Erbacher*, J. (2013). Paleoclimate reconstruction during Mamu formation (Cretaceous) based on clay mineral distributions. IOSR *Journal of Applied Geology and Geophysics* (IOSR-JAGG) e-ISSN: 2321–0990, p-ISSN: 2321–0982, 1(5), pp.40-pp.46.

Ogundipe, I. E. and Obasi, R. A. (2016). Geology and mineralization in the Albian sediments of the Benue Trough, Nigeria. *British Journal of Earth Sciences Research,* 4(3), pp1-pp.15.

Oha, I. A.; Onuoha, K. M.; Nwegbu, A. N. and Abba, A. U. (2016). Interpretation of high resolution aeromagnetic data over Southern Benue Trough, southeastern Nigeria. *Journal of Earth System. Sci.ence, 125(2),* pp.369–pp.385.

Okezie, C. N. (1965). A preliminary report on the igneous rocks of Abakaliki town and its environment and their relation to Lead-Zinc mineralization, Geological Survey Nigeria report no 1348 (Unpublished)

Olade, M. A. (1976). On the genesis of lead-zinc *deposits* in Nigeria's Benue rift (aulacogen); A re-interpretation. *Nigerian. Journal of Mining* Geology, Vol.13, pp.20-pp.27.

Olade, M. A. (1978). Early Cretaceous basaltic volcanism and initial continental rifting in Benue trough. *Nature Physical. Science*, 27(3), pp.458-pp.459.

Olade, M. A and Morton, R. D. (1980). Temperature of ore formation and origin of the Ishiagu Lead-Zinc deposit, Southern Benue Trough. *Nigerian Journal of Mining Geology*, Vol.17, pp.19-pp.127.

Olade, M. A. and Morton, R. D. (1985). Origin of Lead-Zinc mineralization in the Southern Benue Trough, Nigeria: Fluid inclusion and trace element studies. *Mineralum Deposita*, Vol.20, pp.76- pp.80.

O'Leary, D.W; Friedman, J. D and Pohn, H. A. (1976). Lineaments, linear, lineations: Some proposed new standards for old terms. *Geological Society American. Bulletin.* Vol.89, pp.1463-pp.1469.

Omada, J. I. and Echefu, C. I. (1996). On the economic appraisal and genesis of the barite mineralization and saline springs in the Middle Benue Trough, Nigeria. *Journal of Mineralogy, Petrology and Economic Geology*, 91(3), pp.109-pp.115.

Onu, F. K (2017). The Southern Benue Trough and Anambra Basin, South Eastern Nigeria: A Stratigraphic Review. *Journal of Geography, Environment and Earth Science International*, 12(2), pp.1-pp.16, Article no. JGEESI.30416. ISSN:2454-7352.

Onyewuchi, R. A and Ugwu, S. A. (2016). Geological interpretation of the high resolution aeromagnetic data over Okigwe-Udi area, Anambra Basin, Nigeria, using 3D Euler Deconvolution and 2D spectral inversion methods. *Journal of Geography, Environment and Earth Science International,* 10(1), pp.1-pp.22.

Onuba, L. N.; Anudu, G. K.; Chiaghanam, O. I. and Anakwuba, E. K. (2011). Evaluation of aeromagnetic anomalies over Okigwe area, southeastern Nigeria. *Research Journal of Environmental and Earth Sciences*. 3(5), pp.498-pp.507.

Opara, A.I. (2011). Estimation of the depth to magnetic basement in parts of the Dahomey Basin, Southwestern Nigeria. *Australian Journal of Basin and Applied Sciences,* 5(9), pp.335-pp.343.

Opara, A. I.; Ekwe, A. C.; Okereke, C. N.; Oha, I. A. and Nnosiri, O. P. (2012). Integrating airborne magnetic and Landsat data for geological interpretation over parts of Benin Basin, Nigeria. *The Pacific Journal of Science and Technology,* 13(1), pp.556-pp.571.

Orajaka, S. (1965). Geology of Enyigba, Ameri and Ameka Lead-Zinc mines; *The Journal of Geology.,* Vol.3, pp.49–pp.51.

Peters, E. R. (1983). The use of multispectral satellite imagery in the exploration for petroleum and minerals. Phil. Trans. Roy. Soc. London, *Vol. 309, pp.243-pp.255*

.

Petters, S.W. (1978). Stratigraphic evolution of the Benue Trough and its implications for the Upper Cretaceous paleogeography of West Africa. The Journal of Geology. 86(3)*, pp.311–pp.322.*

Pilkington, M and Beiki, M. (2013). Mitigating remanent magnetization effects in magnetic data using the normalized source strength, Geophysics*, Vol.78, pp.25-pp.32.*

Pilkington, M. (1997). Magnetic imaging using conjugate gradients: Geophysics, *Vol.62, pp.1132-pp.1142.*

Planck, M. (1914). The theory of heat radiation. Masius, M. (transl.)(2nd ed. P Blakiston's Son & Co., *Vol. 6, pp.168.*

Prost, G. (2014). Remote sensing for geoscientists: Image Analysis and Interpretation., London: CRC Press, https://doi.org/10.1201/b15638. *ISBN-13:978-1466561748, ISBN-10:1466561742.*

Rajesh (2004). Application of remote sensing and GIS in mineral resource mapping – An overview, Journal of mineralogical and petrological

sciences, 99(3),pp.83-103 *DOI: 10.2465/jmps.99.83.*

Reynolds, R. L.; Rosenbaum, J. G.; Hudson, M. R. and Fishman, N. S. (1990). Rock magnetism, the distribution of magnetic minerals in the earth's crust and aeromagnetic anomalies. United State Geological Survey Bulletin, 1924, pp.24-pp.25.

Robbins, E. I. (1983). Accumulation of fossil fuels and metallic minerals in active and ancient rifts. *Tectonophys*, Vol.94,pp. 633-pp.658.

Rowan, C. C. and Bowers, T. L. (1995). Analysis of linear features mapped in Landsat Thematic Mapper and side-looking airborne radar images of the Reno, Nevada 18 by 28 quadrangle, Nevada and California – Implications for mineral resources studies. *Photogramm. Eng. Remote Sensing,* Vol..61, 749-759.

Ryan,W. B. F.; Carbotte,S. M.; Coplan,J. O.; O' Hara, S.; Melkonian, A.; Arko, R.; Weissel, R. N.; Ferrini,V.; Goodwillie, A.; Nitsche, F.; Bonczkowski, J. and Zemsky, R. (2009). Global multi-resolution topography synthesis, Advancing earth and ppace science: Topographical map of the study area, *Geochemistry. Geophysics. Geosystem*s., 10(3), pp.1-21.Q03014, doi: 10.1029/200).

Sawkins, F. J. (1976). Massive sulphide deposits in relation to geotectonics. In: Strong, D.F (ed) Metallogeny and plate tectonics. Spec. Pap. Geologic Association of Canada Special Paper Vol.14, pp.221-pp.240.

Schmidt, P.; Clark, D. A.; Leslie, K.; Bick, M.; Tilbrook, D. and Foley, C. (2004). GETMAG a SQUID magnetic tensor gradiometer for mineral exploration*: Exploration Geophysics,* .35(4), pp.297-pp.305.

Schowengerdt, R. A. (2007). Remote sensing: Models and methods for image processing (3rd ed.). Academic press. p.2. ISBN 978-0-12-3694007-2.

Sharma, P. V. (1987). Magnetic method applied to mineral exploration; *Ore Geology*, review. 2, pp.323-pp.357.

Sharma, P. V. (1997) Environmental and Engineering Geophysics. Cambridge University Press, UK.

Shearer, S. (2005). Three dimensional inversion of magnetic data in the presence of remanent magnetization: MSc. thesis, Colorado School of Mines and 74th Annual International Meeting, SEG, Expanded Abstracts, pp.774-pp.777.

Sheriff, R. E. (1991) Encyclopedic Dictionary of Exploration Geophysics. Third Edition. *Geophysical References Series 1*. SEG Publication

Tattam, C. M. (1930). Geophysical investigation upon the lead-zinc lodes of Ogoja Province. Geological Survey of Nigeria, Annual Report., pp.14-pp.23.

Telford, W. M.; Geldart, L. P.; Sheriff, R. E and Keys, D. A. (1990). Magnetic Methods. In: Applied Geophysics (Second Edition: Cambridge University Press, Cambridge UK, pp. 344 - pp.536.

Thompson, D. T. (1982). EULDPH: A new technique for making computer-assisted depth estimates from magnetic data. *Geophysics,* Vol.47, pp.31–pp.37.

Uma, K. O; Onuoha, K. M and Egboka, B. C. (1990). Hydrochemical facies, groundwater flow pattern and origin of saline waters in parts of the western flank of the Cross River Basin, Nigeria. In: The Benue Trough, structure and evolution. (eds. C.O. Ofoegbu), pp.115-pp.134; Braunschweig, Vieweg.

Uma, K. O. and Loehnert, E. P (1992). Research on the saline groundwaters in the Benue Trough,

Nigeria: Preliminary results and projections. *Zbl. Geol. Palaont. Teil I, H*. Vol. 11, pp.2751-pp.2756, Stuttgart.

Uma, K. O. (1998). The brine fields of the Benue Trough, Nigeria: A comparative study of geomorphic, tectonic and hydrochemical properties. *Journal of African Earth Sciences. 26(2),* pp.261-pp.275.

Umeji, A. C. and Caen-Vachette, M. (1983). Rb-Sr Isochron from Gboko and Ikyen Rhyolites and its implications for the age and evolution of the Benue Trough, Nigeria. *Geol. Mag.,* Vol. 120, pp.529-pp.533.

Umeji (1988). Trace fossils from Eze-Aku formation (Turonian), Sotheastern Nigeria. *Journal of mining and geology,* 24 (1&2), pp.79-pp.80.

U.S. Geological Survey (2018). Landsat collections, U.S. Geological Survey fact sheet, Vol.2, pp.2018–pp.3049.

Utsugi, M. (2019). 3D Inversion of magnetic data based on L_1-L_2 norm regularization. Earth, Planets and Space, 71(73).

Wilson, H. S. (1985). Analysis of the magnetic gradient tensor, Defence Research Establishment Pacific, Technical Memorandum. Vol.8, pp.5-pp.13.